Marine and Petroleum Geology 138 (2022) 105525

Contents lists available at ScienceDirect

Marine and Petroleum Geology

journal homepage: www.elsevier.com/locate/marpetgeo

Mapping the maturity of organic-rich shale with combined geochemical and geophysical data, Draupne Formation, Norwegian Continental Shelf

James Ronald Johnson [a,*], Jørgen André Hansen [a], MD Jamilur Rahman [a], François Renard [a,b], Nazmul Haque Mondol [a,c]

[a] Department of Geosciences, The Njord Centre, University of Oslo, P.O. Box 1047, Blindern, NO-0316, Oslo, Norway
[b] ISTerre, Univ. Grenoble Alpes, Grenoble INP, Univ. Savoie Mont Blanc, CNRS, IRD, Univ. Gustave Eiffel, 38000, Grenoble, France
[c] Norwegian Geotechnical Institute (NGI), P.O. Box 3930, Ullevaal Stadion, NO-0806, Oslo, Norway

ARTICLE INFO

Keywords:
Norwegian Continental Shelf
Source rock shale
Upper Jurassic shale
TOC
Maturation
Kerogen
Brittleness
Rock physics
Seismic inversion

ABSTRACT

The evaluation of the interplay between kerogen maturation and total organic carbon (TOC) content within an organic-rich shale is critical to characterizing source rock shale's elastic behavior. We analysed a comprehensive database of twenty-nine well logs, two 3D seismic surveys, and geochemical data of eighteen wells within the Draupne Formation in the Norwegian North Sea. The Upper Jurassic (Kimmeridgian) Draupne Formation Shale is found throughout the Norwegian Continental Shelf and is the primary source, carrier, and seal rock in several oil and gas fields. The dataset explores a broad range of depths (2–5 km), total organic contents (0–20 wt%), and various maturation states ranging from immature to overmature. We study the relationship between rock brittleness and organic content as shale matures. We use calculated values of Young's modulus and Poisson's ratio. Academic and industry-standard cutoffs are applied to both the TOC content and maturation level. We introduce here the Organic Maturation Product (OMP) rock physics template, which incorporates a relationship between organic content and any subsequent maturation. The degree of brittleness or ductility is impacted directly by the kerogen maturation process, with lower TOC content having a dampening effect on the transition towards increasing brittleness. This template allows one to classify rock maturation in nine categories, from low to high maturation, and link these categories to rock geomechanical properties. Seismic inversion of the 3D surveys and mapping utilizing the OMP classification reveal how large-scale depositional environment and subsequent diagenetic events influence both placement and quality of source rock broadly within the basin context of the North Sea.

1. Introduction

The exploitation of unconventional shale reservoirs has driven continued interest in the characterization and understanding of their microstructure and their mechanical and hydraulic properties (e.g., Vernik and Landis, 1996; Sonnenberg, 2011; Ewy, 2019; Ougier-Simonin et al., 2016; Kennedy and Mayer, 2019). A benefit of these efforts has been a greater understanding of shales and the importance they have within conventional and unconventional hydrocarbon plays as both source and seal/cap rocks. The maturation of organic-rich shales results in fundamental variations of their geophysical, geochemical, and petrophysical properties (Prasad et al., 2009; Anders et al., 2014). Further to this, the interaction between the amount of total organic carbon (TOC) content and kerogen maturation will directly impact the organic-rich shale's quality as a source and cap rock (Hansen et al., 2020; Rahman et al., 2020).

The Upper Jurassic (Kimmeridgian) Draupne Formation (Fig. 1b) is a world-class source rock and an effective seal in the Central and Northern North Sea. This formation stretches over a broad range of depths (500–6500 m), thicknesses (0–550 m), TOC, and maturity (NPD, 2021). It provides an ideal candidate to study the interplay between kerogen maturation and TOC content. In the Southern North Sea, the equivalents to the Draupne Formation are the Mandal and Tau Formations, which vary in thickness ranges 1–170 m for the Mandal Formation) and 2–118 m for the Tau Formation. In the Norwegian Sea and the Barents Sea, the equivalents to the Draupne Formation are the Spekk and Hekkingen Formations, which vary in thickness range 1–150 m for the Spekk Formation and 2–190 m for the Hekkingen Formation (NPD, 2021).

* Corresponding author.
E-mail address: j.r.johnson@geo.uio.no (J.R. Johnson).

https://doi.org/10.1016/j.marpetgeo.2022.105525
Received 21 September 2021; Received in revised form 17 December 2021; Accepted 3 January 2022
Available online 6 January 2022

Mapping how the Draupne Formation varies across the Norwegian North Sea is an important task that is made difficult by the size of the basin compared to the number of wells, consistency of the quality of data, and the relative dimension of seismic surveys to the size of the basin. A relationship between maturation and geomechanical properties represented by alterations in brittleness of organic-rich shale has been proven (Prasad et al., 2011; Zargari et al., 2016). Besides, a relationship between TOC content and geomechanical properties has been the topic of many studies, with sometimes contrary conclusions (Grieser and Bray, 2007; Wilson et al., 2017, Mondol, 2018). One group concludes that an increase in TOC correlates to an increase in brittleness (Grieser and Bray, 2007; Wilson et al., 2017), while another group shows that increased TOC correlates to increased ductility (Mondol, 2018). Here, we study the interaction between TOC and kerogen maturation in relationship to seismic velocity and elastic parameters. While the use of correlations between elastic properties and brittleness parameters is debated (Thomsen, 1990, 1996; Holt et al., 2015), it remains a useful tool to approximate geomechanical properties.

Here, we seek to understand how TOC and maturation can vary both in terms of depositional and diagenetic characteristics in the Draupne Formation. To reach this goal, we use mapping of two specific sections of the basin and utilize 3D seismic surveys at different depths and locations. Knowledge of TOC and maturation differences are initially built upon rock physics templates to compare a broad range of well log data in terms of both depth and shale thickness. The dataset is further supported by geochemical data, primarily based upon cuttings analysis of geochemical reports produced by the Norwegian Petroleum Directorate ((NPD, 2021). We introduce a rock physics template called the Organic Maturation Product (OMP) and demonstrate its utility in clarifying the relationship between the net amount of organic content and any subsequent maturation. OMP is also used to characterize the impact of salt diapirism upon maturation.

2. Geological setting

The study area contains structural elements of the Ling Depression, Utsira High, Patch Bank Ridge, and Gudrun Terrace that constitute the main geological structures in the Central North Sea Basin (Fig. 1). Exploration and development in the region have been variable, with more data coming from areas that have had greater economic success. The study area includes the Sleipner Vest and Sleipner Øst fields, providing significantly more data where the study area overlaps with these fields.

Two major rifting events occurred in the Norwegian North Sea (Ziegler, 1992; Faleide et al., 2008). The first rifting event occurred in the Triassic, followed by post-rifting tectonic quiescence. The second rifting event that occurred in the Late Jurassic – Early Cretaceous in the North Sea formed significant structural relief (Whipp et al., 2014). This rifting event, coupled with eustatic sea-level rise, resulted in anoxic, restricted environments. Subsequent uplift and erosion regionally have resulted in lateral variations of sediment thickness across the region, perhaps most significant during the Barremian (Bugge et al., 2001; Isaksen and Ledje, 2001; Faleide et al., 2008; Hansen et al., 2017). Uplift of the Mid-North Sea Dome during the Early Jurassic resulted in subsequent nondeposition in certain areas (Ziegler, 1992; Mannie et al., 2014). Further complicating the geological history, major salt deposition occurred during the Permian in the Norwegian Continental Shelf (Jackson et al., 2010; Rossland et al., 2013). Subsequent passive salt diapirism was shown to impact the structure of the overlying Jurassic-Cretaceous age deposits, including the Draupne Formation around the Utsira High and the Ling Depression (Jackson et al., 2010; Johnson et al., 2021). The salt's thermal properties can significantly alter thermal gradient (Daniilidis and Herber, 2017), which in turn can have an impact on kerogen maturation and the rate of maturation of organic-rich shale (Johnson et al., 2021).

The Draupne Formation within the Viking Group, part of the Upper Jurassic, is an organic-rich shale formation equivalent to the Kimmeridgian Shale in the UK sector. The formation consists of dark grey-brown to black, usually non-calcareous claystone, that is occasionally fissile in nature (NPD, 2021). The mineralogy for the Draupne Formation is dominated by clays and organic matter. The average clay content for the Draupne Formation from these studies, within our study area, is 66 ±

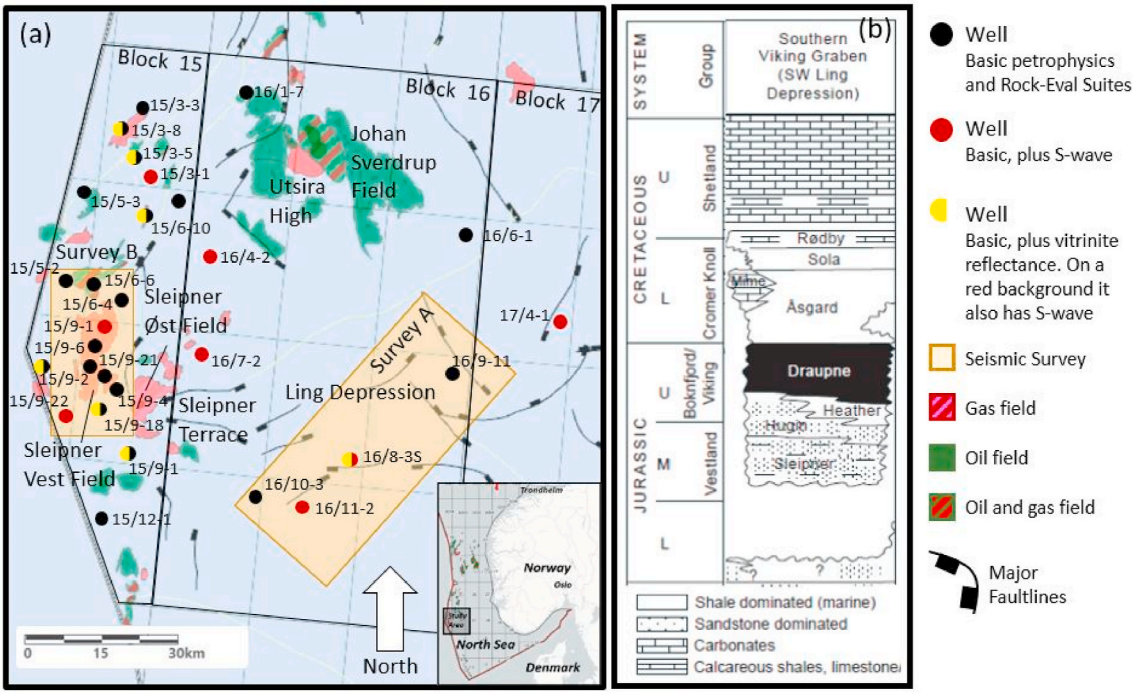

Fig. 1. (a) Map of the study area, including all 29 wells with varying amounts of information, both petrophysical and Rock-Eval suites as defined in the legend, and the locations and relative sizes of the two 3D seismic surveys utilized (Surveys A and B) (b) Stratigraphy of the Draupne Formation and the underlying and overlying formations deposited during the Early Jurassic to Late Cretaceous (modified from NPD, 2021).

4%, the average quartz and feldspar content is 21 ± 5%, and the average carbonate and pyrite content is 13 ± 1% (Kalani et al., 2015; Skurtveit et al., 2018; Nooraiepour et al., 2017; Zadeh et al., 2017; Hansen et al., 2020; Johnson et al., 2021). The total depth range for the Draupne Formation from penetrated well in the Norwegian North Sea is from ~500 to 6500 m depth, while thickness ranges from ~0 to 550 m (NPD, 2021). While TOC can reach upwards of 20 wt% in the Draupne Formation (Løseth et al., 2011), a more typical range is from 2 to 15 wt%. Due to a broad range in depth, TOC richness, and maturity, the hydrogen index (HI) can vary significantly (present study, Hansen et al., 2019). Another characteristic of the Draupne Formation in some regions of the North Sea is intermittent quartz-rich sandstone sections resulting from sporadic debris flows or turbidites that broke up the deposition of the clay-rich sections (Bugge et al., 2001; Isaksen and Ledje, 2001). While the formations Tau, Sauda, Egersund, and Heather also have source rock potential (Fig. 1b), the quality is poorer and significantly more variable (Hansen et al., 2019); as such, they were not included in the present study.

3. Database and methods

Two three-dimensional (3D) seismic datasets, named A and B, have been used alongside a selected database of twenty-nine exploration wells based on the location, depth, and thickness of the Draupne Formation (Fig. 1). The Draupne Formation depth in our study area is ~2.0–5.0 km, while the thickness is 20–800 m (Table 1). Seismic survey A covers a large swathe of the Ling Depression and a portion of the Sele High, while survey B covers a part of the Sleipner Terrace and then extends west towards the Norway-UK maritime border. Survey A is roughly four times the size of Survey B (Fig. 1). Despite the difference in sizes, both datasets provide insight into the Draupne Formation showing regions with large thickness, depth, and maturity variations. Mapping out both surveys also allows for broader depositional and diagenetic trends influencing the Draupne Formation to be inferred.

Well data consisted of both petrophysical well log measurements in addition to geochemical data acquired in the laboratory on rock samples along with the wells (Table 1). All well data contained petrophysical

Table 1
Overview of the twenty nine (29) exploration wells included in the database, the depth and thickness of the Draupne Formation. Well logs and Rock-Eval data available for each well are indicated. Logging data are Kelly Bushing (KB), Gamma Ray (GR), P-sonic (Vp), S-sonic (Vs), Hydrogen Index (HI), Oxygen Index (OI), Temperature Max (Tmax), Vitrinite Reflectance (VR), Production Index (PI), and Total Organic Carbon (TOC).

Well (prospect/ field)	Content	Draupne Top KB (km)	Draupne Thickness (m)	GR	Vp	Vs	Density	Resistivity	Neutron Porosity	HI	OI	Tmax	VR	S2	TOC (measured)
15/3–1 (Gudrun)	Gas/ Cond	3.84	807	X	X	–	X	–	X	–	–	X	X	–	X
15/3-3 (Gudrun)	Gas/ Cond	3.91	208	X	X	–	X	X	X	X	X	X	–	–	X
15/3–5(Sigrun)	Oil	3.70	73	X	X	X	X	–	X	X	X	X	X	X	X
15/3–8 (Gudrun)	Oil/Gas	3.82	222	X	X	X	X	X	X	–	–	–	–	–	–
15/5–2 (Eirin)	Gas	3.64	72	X	X	–	–	X	–	X	X	X	–	–	X
15/5-3	Oil Shows	3.56	135	X	X	–	–	X	–	X	X	X	–	–	X
15/6-4	Dry	3.05	30	X	X	–	–	X	–	X	X	X	–	X	X
15/6-6 (Sleipner Vest)	Gas/ Cond	3.28	20	X	X	–	X	X	X	X	X	X	–	–	X
15/6–10 (Freke)	Gas/ Cond	3.35	36	X	X	X	X	X	X	–	–	–	–	–	–
15/8-2	Dry	3.65	76	X	X	X	X	X	X	–	–	–	–	–	–
15/9–1 (Sleipner Vest)	Oil/Gas	3.27	108	X	X	–	X	X	X	–	–	–	X	–	X
15/9–2 (Sleipner Vest)	Gas/ Cond	3.29	82	X	X	–	X	X	X	X	X	X	–	–	X
15/9–4 (Sleipner Vest)	Gas/ Cond	3.17	147	X	X	–	X	X	X	–	–	–	–	–	–
15/9–6 (Sleipner Vest)	Dry	3.36	230	X	X	–	X	X	X	–	–	–	–	–	–
15/9–11 (Sleipner Øst)	Gas/ Cond	2.66	14	X	X	X	X	X	X	X	X	X	X	X	X
15/9-18	Dry	3.01	105	X	X	–	X	X	X	–	–	–	–	–	–
15/9–21 (Sleipner Vest)	Dry	4.32	269	X	X	–	X	X	X	–	–	–	–	–	–
15/9-22	Dry	3.30	148	X	–	–	–	X	–	X	X	X	X	X	X
15/9-23	Dry	2.86	100	X	X	X	X	X	X	–	–	–	–	–	–
15/12-1	Oil Shows	2.91	23	X	X	–	X	X	X	X	X	X	–	X	X
16/1–7 (Ivar Aasen)	Oil	2.64	171	X	X	–	X	X	X	X	X	X	X	X	X
16/4-2	Dry	2.87	152	X	X	–	X	X	X	X	X	X	–	X	X
16/6-1	Dry	1.90	32	X	X	–	X	X	–	X	X	X	–	–	X
16/7-2	Gas	2.50	89	–	X	–	X	X	X	X	X	X	X	X	X
16/8-3S (Lupin)	Dry	2.50	86	X	X	X	X	X	X	X	X	X	–	X	X
16/9-1	Dry	2.21	169	X	X	–	X	X	–	–	–	–	–	–	–
16/10-3	Dry	2.43	20	X	X	–	X	X	–	X	X	X	–	X	X
16/11-2	Dry	2.06	75	X	X	–	X	X	–	X	–	–	X	X	X
17/4–1 (Vette)	Dry	2.02	95	X	X	–	X	X	X	X	X	X	X	–	X

measurements that include the typical suite of wireline logs such as gamma ray (GR), bulk density (ρ), neutron porosity, resistivity (R), and P-wave velocity (Vp). Among the twenty-nine wells, only seven of them contained S-wave velocity (Vs) data. There was a wide range in the vintages of well logs, ranging from 1967 to 2013, with ~80% of the wells from the 1960s–1990s (NPD, 2021). Sonic logs were de-spiked and filtered to remove and correct for anomalous data points. Additionally, all well logs were checked for artifacts from washouts, casing points, and mud filtrate invasion. Corrections were made where they were required. Finally, all well logs were normalized to determine appropriate ranges and cutoffs. Note, most corrections that were applied occurred outside of the Draupne Formation and therefore had no material impact on the study. Geochemical data were also available through Rock-Eval and optical reflectance measurements for eighteen out of the twenty-nine wells. The amount of data and data type available varied greatly between wells, possibly including Hydrogen Index (HI), Oxygen Index (OI), TOC, S2, T_{max}, and vitrinite reflectance (R_o). Here, S2 represents the amount of hydrocarbons generated through the thermal cracking of nonvolatile organic matter.

Efforts were made to fully utilize the available dataset; however, there were several inherent limitations presented by both the type and quality of data. The seismic datasets allow for the estimation of P-Impedance and S-Impedance; however, angle limitations (~40°) for both datasets prevent the use of density. Further to this, anisotropy information is not available for either seismic cube, which limits the geomechanical interpretations possible for shale with the seismic data (Sayers and Dasgupta, 2019). If well log data available were plentiful, the study would have benefitted from nuclear spectroscopy logs, which could have been used to directly estimate the TOC and mineralogy (Craddock et al., 2019).

The mineralogical composition has an impact on brittleness. In shales, the content of soft components (clay minerals, TOC) and stiff components (quartz, feldspar, carbonate, pyrite) control brittleness (Jarvie et al., 2007; Jin et al., 2014; Alzahabi et al., 2015; Bourg, 2015). The acccumulations of microquartz, which precipitates at around 80 °C, may increase brittleness (Thyberg et al., 2009). Avseth and Carcione (2015) highlight that the presence of calcitic beds interbedded with the Draupne Formation near the Horda Platform would also increase brittleness. On the other side, Bourg (2015) argues that shale behavior will be inherently ductile above a threshold of 34% clay content. With a clay content of ~66%, the Draupne Formation exceeds this threshold, and in Bourg (2015) the Draupne Formation had one of the highest clay contents investigated. While clay mineralogy is of secondary importance to overall mineralogy in terms of brittleness (Rahman et al., 2020), it has been shown that clay mineralogy can have an impact on brittleness and even the behavior of faults (Haines et al., 2009; Soto et al., 2021).

In addition to mineralogy, pore pressure and fluid effects are also known to have an impact on the brittleness of organic-rich shales (Cook, 1999; Nygård et al., 2006). Increases in pore pressure will cause an increase in brittleness (Nygård et al., 2006), which can have an impact on the integrity of a shale formation (Rahman et al., 2020). Maturation transforms brittle kerogen lenses into hydrocarbons (Chauve et al., 2020). The expulsion of fluids will have an impact on the pore fluid pressure in the shale, which is controlled by the rate of expulsion, compared to the ability of the shale to either absorb or expulse the fluid to surrounding formations (Wu et al., 2016). The expulsion of fluids to surrounding formations will be directly impacted by the degree of microfracture creation linked to hydrocarbon expulsion (Chauve et al., 2020).

3.1. Reference rock physics analysis

Rock physics analysis presented here is based on well log data and separated into two basic templates. We selected these templates to investigate the relationship between elastic properties and TOC, as well as influences on maturation. The first template is a crossplot of P-wave velocity with bulk density utilized for both simplicity and consistency. Additionally, the results and the conclusions drawn from these data are the same for this dataset when compared to a P-wave velocity with S-wave velocity crossplot. As a result, we will focus on P-wave velocity with bulk density crossplots. The second template utilized is a cross plot between Young's modulus and Poisson's ratio. Poisson's ratio contains information of P- and S-wave velocities, while Young's modulus contains information on bulk density in addition to the other two. Young's modulus and Poisson's ratio were calculated using Equations (1) and (2) (Zoback, 2007):

$$\upsilon = \frac{V_p^2 - 2V_s^2}{2V_p^2 - 2V_s^2} \tag{1}$$

$$E = \rho V_s^2 \frac{3V_p^2 - 4V_s^2}{V_p^2 - V_s^2} \tag{2}$$

where υ, E, Vp, Vs, and ρ are Poisson's ratio, Young's modulus, P-wave velocity, S-wave velocity, and density, respectively. The two rock physics templates utilize three independent properties: P-wave velocity, S-wave velocity, and bulk density. However, by combining and displaying these three parameters in different ways, one can highlight different rock properties. For example, the cross-plot between P-wave velocity and either density or S-wave velocity is used to differentiate broadly between lithologies (Gardner et al., 1974; Castagna et al., 1985). Poisson's ratio and Young's modulus can be crossplotted in order to investigate the ductility or brittleness of rock (e.g., Perez and Marfurt, 2014). Young's modulus is a proxy for a rock's brittleness, with a built-in assumption that a higher value will correspond to a greater required applied stress to induce a given strain (Fox et al., 2013), while Poisson's ratio describes lateral expansion to axial contraction (e.g., Fjaer et al., 2008). When calculating Young's modulus and Poisson's ratio, one must remember that they are calculated utilizing both P- and S-wave velocities (Equations (1) and (2)). As such, they are not perfect representations of their laboratory counterparts (Thomsen, 1990, 1996).

Further to this, brittleness in itself is a broadly defined term (Holt et al., 2015). Jarvie et al. (2007), among others (Glorioso and Rattia, 2011; Jin et al., 2014; Alzahabi et al., 2015) relate brittleness to mineralogy directly (MBI), utilizing variations on the equation:

$$\mathrm{MBI} = \frac{\mathrm{Qtz} + \mathrm{Carb} + \mathrm{Fsp} + \mathrm{Py}}{\mathrm{Qtz} + \mathrm{Carb} + \mathrm{Fsp} + \mathrm{Py} + \mathrm{Cly} + \mathrm{TOC}} \tag{3}$$

where Qtz is quartz (wt%), Carb is carbonate (wt%), Fsp is feldspar (wt %), Py is pyrite (wt%), Cly is total clay (wt%), and TOC is total organic carbon (wt.%). MBI ranges between 0 (ductile) to 1 (brittle) and increases with increasing brittleness. As previously stated, mineralogy data are not available for many wells in our study area. However, the MBI range given by bulk mineralogy analysis from other studies within the area (Kalani et al., 2015; Skurtveit et al., 2018; Nooraiepour et al., 2017; Zadeh et al., 2017; Hansen et al., 2020; Johnson et al., 2021) is confined to 0.18–0.28 based on Equation (3). This confirms that the Draupne Formation would be considered ductile utilizing this method, and that it would plot within a narrow window for the study area.

An alternative definition for brittleness is based on elastic properties (EBI), utilizing calculated values of Young's modulus and Poisson's ratio. Grieser and Bray (2007) provide an empirical equation for this approach:

$$\mathrm{EBI} = \frac{1}{2}\left[\frac{E - E_{min}}{E_{max} - E_{min}} + \frac{\nu - \nu_{max}}{\nu_{min} - \nu_{max}}\right] \tag{4}$$

where E is the static Young's modulus, E_{max} is 69 GPa, E_{min} is 0 GPa, ν is the static Poisson's ratio, ν_{max} is 0.5, and ν_{min} is 0. Also, the higher the EBI value is, the more brittle the caprock is. Given data availability, and the nature of the dataset, the present study focuses on the elastic approach to brittleness. Therefore, we use the template provided by

Perez and Marfurt (2014). This template has been widely utilized in geomechanical studies (e.g., Gray et al., 2012; Johnson, 2017; Hansen et al., 2020) and applied to shale reservoirs, caprocks, and seals alike.

This template was calculated for the eighteen wells where Vs data were not available. A comparison was made between Castagna et al. (1985) empirical method and an empirical relationship between Vp and Vs. While both methods are imperfect, based on a blind well test, the empirical relationship estimated purely from Vp was more accurate and therefore used for the present study. However, it was only utilized as a point of comparison to the seven wells with available Vs data and as an independent verification against the two seismic inversion's results. Thereby, the Z-axis is used on both of the rock physics templates to investigate how the rock properties vary with depth, temperature, porosity, and TOC content, respectively. Porosity and depth were taken directly from the well logs. Temperature (^{o}C) was taken from recorded bottom-hole temperatures (BHTs) and then extrapolated for all of the data points based on a depth-temperature curve established from all of the wells (Equation (5)) with a high R^2 value of 0.9.

$$T = 0.031d + 20.8 \tag{5}$$

where T is temperature measured in degrees Celcius and d is depth measured in meters. Temperature is not Horner (1951) corrected, as the data required to do so are rarely available. However, it appeared to confirm the trend established where data were available. TOC was calculated in various ways and compared for the results that best match the laboratory values of TOC. The ΔlogR method utilizes sonic and resistivity logs (Passey et al., 1990, 2012), while both Schmoker and Hester (1983), as well as Vernik and Landis (1996), proposed density-based methods. Further to these, Heslop (2010) proposed a method that utilizes gamma ray and deep resistivity logs. While all methods matched the data well, we found that the density-based approach by Schmoker suited the results best. A high R^2 value of 0.95 was found between the calculated and measured data.

3.2. Seismic inversion workflow

The seismic datasets were all processed prior to receiving them, and we inspected them to ensure they matched the criteria for successful seismic inversion (Yilmaz, 2001). Both Hampson-Russell and Jason Geoscience Workbench softwares were used for the inversions. Survey A is post-stack data, while Survey B is pre-stack data. For both seismic surveys, velocity models were created or improved upon utilizing sonic curves and Vertical Seismic Profiles (VSPs). Improving the velocity models was assisted in part by confirming horizons with an extensive 2D seismic line network. The velocity models were later improved through the horizon picks and the well-ties as part of the seismic inversion process. The 3D seismic datasets show a variation in depth and thickness. Both datasets had sufficient seismic coverage (i.e. frequency range, fold) for the Draupne Formation. The processing for both seismic cubes was completed to preserve amplitudes and was consistent with what is required for post- and pre-stack inversion and amplitude versus offset/angle (AVO/AVA) analysis (Yilmaz, 2001). Analysis of frequency content for both cubes revealed similar qualities, with frequency ranges from 4 to 70 Hz. Seismic artifacts, which can be due to either acquisition or processing, correspond to coherent anomalies (Galbraith and Hall, 1997; Marfurt and Alves, 2014). They were identified and removed where possible. Cross-equalization of the surveys was carried out to compare the two surveys (Rickett and Lumley, 1999; Baytok and Pranter, 2013). Wavelet equalization was not critical as a comparison between wavelets in the two datasets revealed no major deviation in the reflective character of the Draupne Formation.

After a rock physics review of the well logs, a critical step for successful inversion, one can proceed with the inversion itself. A three term, Aki-Richards, constrained sparse-spike inversion (CSSI) was utilized for this study as it sets the correct absolute impedance range but does not depend directly on the impedance log information (Russell, 1988; Duenas, 2014). The objective function (Equation (6)) for CSSI outlines the core constraints that the user attempts to minimize. For the most accurate representation of the subsurface model, it is best if the inversion relies on the fewest number of free parameters as possible because of the non-uniqueness inherent to the problem (MacFarlane, 2014).

$$\mathrm{F}(V_p, V_s, \rho) = \sum \left(F_{seismic} + F_{contrast} + F_{trend} + F_{spatial} + F_{SVD} + F_{Gardner} + F_{mudrock}\right) \tag{6}$$

where each term represents a misfit function that has been calculated for each seismic trace as a function (F) of the three basic parameters that result from seismic inversion: P-wave velocity (V_p), S-wave velocity (V_s), and bulk density (ρ). Specifically, $F_{seismic}$ controls the seismic residuals, $F_{contrast}$ ensures the solution is sparse by controlling the parameter variance, F_{trend} stabilizes the frequencies related to the trend, $F_{spatial}$ controls the smoothness of the output, F_{SVD} (singular value decomposition) stabilizes the inversion, $F_{Gardner}$ constrains the density, and $F_{Mudrock}$ constrains the S-wave velocity component. Note, accurate Gardner and mudrock trends (Gardner et al., 1974; Castagna et al., 1985) are critical inputs and part of why the rock physics templates used here were chosen. Joint facies-impedance inversion which uses local, facies dependent depth trends (Kemper and Gunning, 2014; Somoza et al., 2015) and supervised machine learning derived depth trends (Yenwongfai et al., 2019) were not investigated here. Joint-facies-impedance inversion updates the low-frequency model through an iterative approach resulting in optimized facies models and elastic properties (Kemper and Gunning, 2014). Supervised machine learning, while relatively new is an approach being further investigated in the literature (Yenwongfai et al., 2019).

A low-frequency model accomplishes two critical goals (1) it accurately represents the well data, and (2) it accounts for the missing low-frequency information not present in the seismic data (Kumar and Negi, 2012). A simple low-frequency model was used with five different methods tested within the software Jason Geoscience Workbench: inverse distance weighted, locally weighted, triangulation, natural neighbor, and global kriging. Global kriging uses a linear combination of weights applied to known data based on a model of spatial correlation, in which the global mean frequency is based on all of the control points (Sheriff, 2002). Well tie and wavelet estimation were carried out for all wells within both surveys. An inverse wavelet, typical for the North Sea (Cox et al., 2020), with a phase of 180° was found for all wells. The time-depth relationships for each well-tie showed little variation suggesting no major alterations due to the stretch-squeeze process. A comparison of seismic data with synthetic traces reveals a strong correlation suggesting reliable seismic inversions for both surveys. Signal-to-Noise Ratio (S/N) was shown to be high for all stacks suggesting good seismic quality. Key parameters for the inversion (Equation (6)) and the rock physics review are shown in Table 2. After initial data

Table 2
Overview of inversion parameters for both 3D seismic surveys. SVD is singular value decomposition.

Parameter	Survey A (value)	Survey B (value)
Window	Draupne FM	Draupne FM
Gardner Slope	0.30	0.30
Mudrock Slope	0.86	0.86
Contrast misfit P-Impedance uncertainty (%)	1	1
Contrast misfit S-Impedance uncertainty (%)	5	5
Contrast misfit Density uncertainty (%)	10	10
Seismic misfit S/N ratio average	18	12
Relative SVD threshold (%)	1	1
Wavelet scale factor	1	1
Merge cutoff frequency (Hz)	4	4

quality control, the workflow for the seismic inversion is shown in Fig. 2.

Finally, the most critical external review is a blind well test, which compares how well the inversion predicts the seismic wave velocities and elastic properties of a well that has not been included in the inversion process. To do this test, we extracted a pseudo-well at the same location as the blind well from the inversion results. In turn, the pseudo-well results were crossplotted with the actual elastic properties from the blind well. An improvement upon this method included pseudo-wells at the same location as the wells involved in the inversion process, in addition to the blind well (Fig. 3). A comparison of all of these results, with a good correlation, was indicative that the petrophysical and seismic inversion results mirror one another. A significant improvement resulted for the S-Impedance, while P-Impedance slightly degraded.

3.3. Quantity of organic material and maturation thereof (organic maturation product)

We have obtained maturation trends by utilizing geochemical data. These data also provided baseline knowledge of the source rock shales and the hydrocarbon therein, including kerogen type and organic content variations. Note that while there is usually an abundance of points taken for the whole well from cuttings, focusing solely on the Draupne Formation severely cuts the number of potential data points per well. Vitrinite reflectance (R_0) data provides the best proxy for maturation (Tissot and Welte, 1984) where available. However, there were fewer initial datapoints for vitrinite reflectance (R_o) available within our study than there were for other data types, including but not limited to Hydrogen Index, TOC, and T_{max}. This is not an uncommon problem with Rock-Eval datasets, especially for the North Sea (NPD, 2021; Sadeghtabaghi et al., 2020). Subsequently, the limited numbers of vitrinite reflectance data were further reduced due to the high uncertainty values present in some of our samples. Also, geochemical data were quality controlled with the specific intention of culling maturity data with low TOC (<2 wt %) or low S2 values (<5 mg HC/g rock) for the calculations with T_{max}, HI, and OI as they are not representative of the Draupne Formation as a whole. Here, S2 represents the amount of hydrocarbons generated through thermal cracking of nonvolatile organic matter. Despite these uncertainties, crossplotting of depth and vitrinite reflectance provided insight into the maturation level. Vitrinite reflectance can be quantified, where there are fewer data points, with the interpretation of hydrogen index (HI) versus TOC. While crossplotting hydrogen index (HI) and T_{max} can provide insight into maturation, one can also confirm kerogen type with this plot (Banerjee et al., 1998). Finally, kerogen type can also be investigated using cross-plots of S2 versus TOC (Espitalie et al., 1985).

A linear relationship can be identified between maturation and depth, with an R^2 value of 0.73 (Fig. 4). The empirical relationship that correlates depth (d) in meters with vitrinite reflectance (R_o) for this region is given by:

$$R_0 = \frac{d}{6181.2} + 0.04 \tag{7}$$

where vitrinite reflectance is represented as a mean R_0 value based on all vitrinite particles measured for a given sample, and depth is represented in meters. However, recognizing that the slope of the trendline within a linear system was different depending on the depth provided the opportunity to view it as potentially exponential. The analysis indicates that an exponential relationship, representative of the chemical kinetics of thermal maturation, may better fit the empirical data. The value of R^2 for the empirical exponential law relationship is 0.82, while the empirical relationship is as follows:

$$R_0 = e^{\left(\frac{d}{3921.4} - 1.41\right)} \tag{8}$$

While the relationship between vitrinite reflectance and depth (Fig. 4) shows that our estimate is close to the regional trend (Baig et al., 2019), it is also true that both for the study area and within the Norwegian North Sea vitrinite reflectance data can be limited. So while a clear trend exists, due to the limited number of vitrinite reflectance datapoints and the quality thereof, the estimation of vitrinite reflectance utilizing a crossplot of hydrogen index (HI) with measured TOC from Vernik and Landis (1996) is used for this study. The trendlines are best representative of type II and III kerogen (Vernik and Landis, 1996), which this dataset predominantly contains, discounting some data from well 15/9–11 and limited data from well 15/3–1. First, the results were

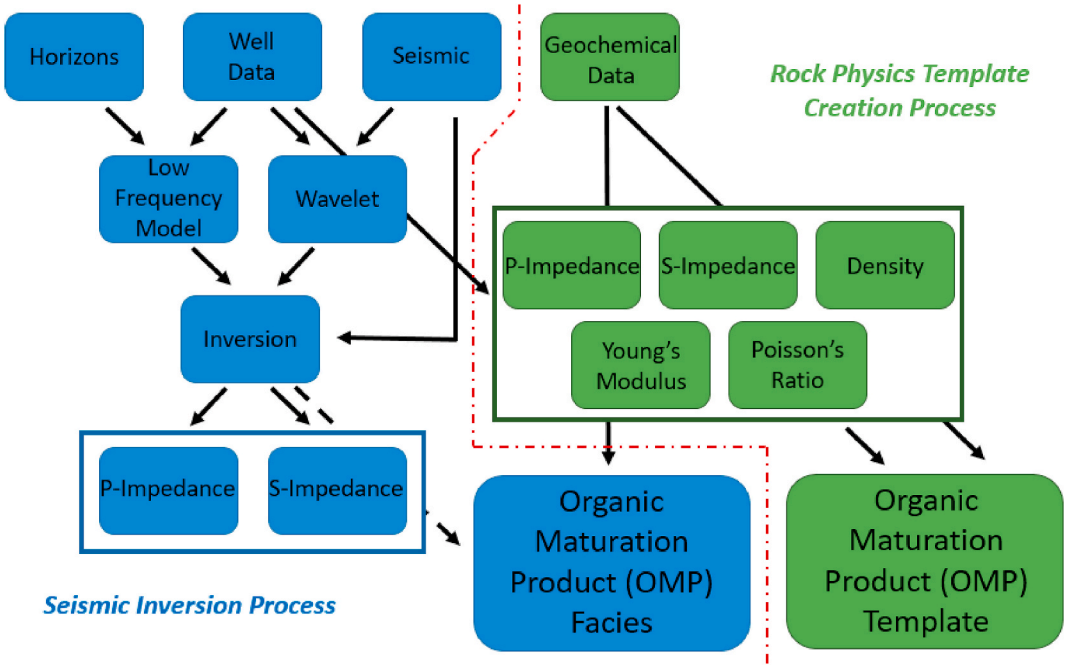

Fig. 2. Workflows implemented for the seismic inversion (blue) and for the creation of the Organic Maturation Product (OMP) rock physics template (green) that describes the relationship between seismic velocities and elastic parameters that accounts for geochemical data.

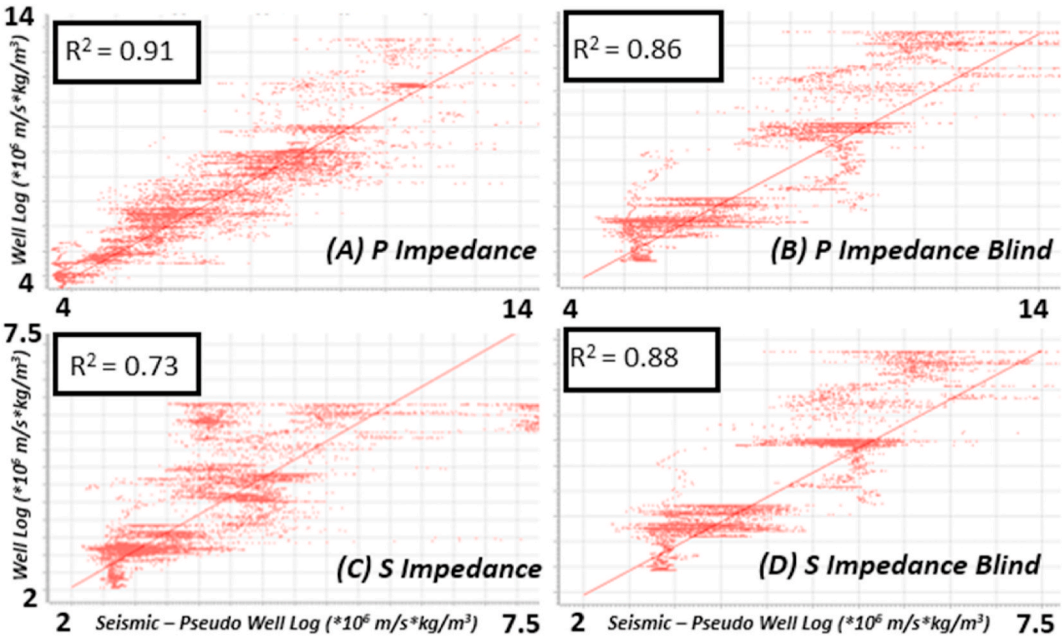

Fig. 3. Seismic and well log comparison with and without blind wells. A comparison of impedance calculated from well logs (y-axis) and pseudo-logs (x-axis) extracted from Survey B shows strong correlations between them for both P-Impedance (a) and S-Impedance (c). A comparison with a blind well is calculated as an additional quality check, revealing a comparably good correlation for P-Impedance (b) and S-Impedance (d).

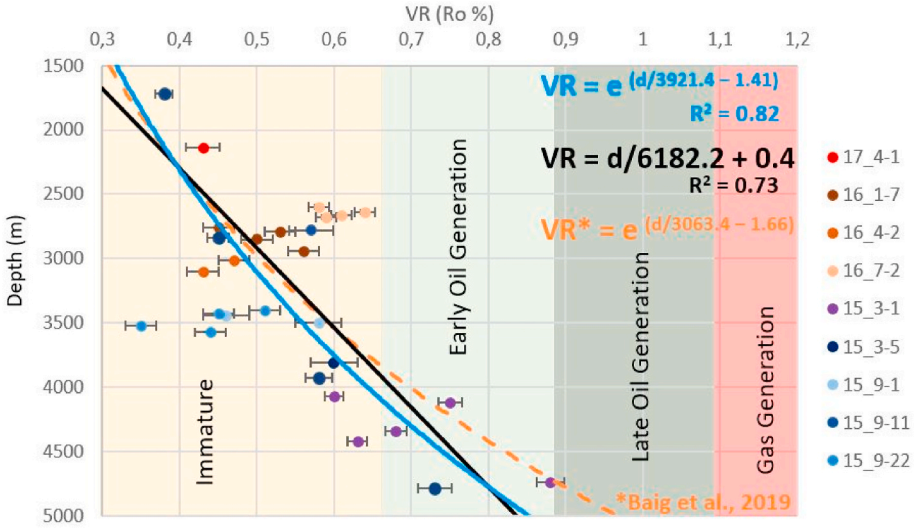

Fig. 4. Crossplot of depth (m) versus vitrinite reflectance (Ro %) showing a relationship between maturation and depth for the study area with three different trendlines applied. The blue trendline shows the relationship as an exponential function, while the black trendline shows it as a linear trend. The green dashed trendline shows the relationship from Baig et al. (2019) which was based on an extensive study on the Norwegian North Sea. (For interpretation of the references to color in this figure legend, the reader is referred to the Web version of this article.)

divided into three categories with regards to TOC, low (<2 wt %), medium (2–5 wt %), and high (>5 wt %). Utilizing the vitrinite reflectance trendlines, the data were further classified into immature, early mature oil generation, late mature oil generation, and gas generation. Table 3 summarizes the combinations of these categories.

The TOC (wt %), to a large degree, determines the potential quantity of expelled hydrocarbon. Low TOC, or low potential hydrocarbon, was determined to be 2 wt% based on accepted industry and academic standards (Kuuskraa et al., 2013; Cooke, 2014; Steiner et al., 2016). Where there is a deviation from this number, it remains ±0.5 wt%. Regionally, Hansen et al. (2019) established that a significant amount of the source rock for the Draupne Formation and surrounding source rocks have a TOC ranging from 5 to 12 wt%. TOC above 5 wt % is considered to be top tier by Beaumont and Foster (1999). Here, it was considered that 5 wt% defines the cutoff between medium TOC and high TOC. While rocks with higher TOC have greater hydrocarbon potential, this parameter does not alone guarantee hydrocarbon expulsion. Maturation, as defined through its proxy vitrinite reflectance, is another control parameter of expulsion. The trends established by Vernik and Landis (1996) were used to estimate vitrinite reflectance values, which were in turn, used to define if hydrocarbon expulsion occurred.

Seismic facies were produced based on the Organic Maturation Product (OMP) facies. To do this, two distinct, discrete background models were created utilizing Bayesian theory to generate probability volumes from the inversion results (Pendrel et al., 2006). The first discrete model separated TOC into the three distinct classes discussed above. The second discrete model separated maturation, as vitrinite reflectance was estimated from the crossplot of hydrogen index and TOC, into the four classes discussed above. In order to combine them, we took the product of TOC as a discrete model and its maturation as a discrete model, i.e., the Organic Maturation Product (OMP), as shown in Table 3 and represented in Equation (9).

Table 3
The Organic Maturation Product (OMP) facies contains nine classes defined based on two components, TOC and maturation, as estimated using vitrinite reflectance (VR).

Organic Maturation Product Facies	Total Organic Carbon (TOC wt.%)	Vitrinite Reflectance (VR % Ro)
Low TOC	<2	–
Medium TOC, Immature	2–5	<0.5
Medium TOC, Early Oil Generation		0.5–0.75
Medium TOC, Late Oil Generation		0.75–1.3
Medium TOC, Gas Generation		>1.3
High TOC, Immature	>5	<0.5
High TOC, Early Oil Generation		0.5–0.75
High TOC, Late Oil Generation		0.75–1.3
High TOC, Gas Generation		>1.3

$$OMP = TOC_{discrete\ model} * Maturation_{discrete\ model} \quad (9)$$

Discrete models create a relationship between calculated elastic properties, in this case, P-Impedance and S-Impedance, and other calculated rock properties. The other calculated rock properties here are TOC and maturation, which have cut-off values assigned based on industry and academic standards as previously discussed. Prior probabilities were then calculated for each discrete model's different components for both seismic Surveys A and B based on the well logs. Finally, probability distribution functions (PDFs) were used to separate the components of each discrete model in a crossplot of P-Impedance and S-Impedance. Fig. 5 displays an example of the product of this workflow, where data in well 15/9–18 have been classified into its discrete components TOC and maturation. The result, the Organic Maturation Product, for well 15/9–18 can be seen overlaid onto the Organic Maturation Product of seismic traces from Survey B around that well. The result is a classification of rock maturation property into nine different classes and provides a way to characterize better the interaction between TOC and maturation in organic-rich shales. Additionally, the mapping of the OMP allows one to investigate depositional and diagenetic impacts simultaneously.

4. Results

The results of our investigation are based on geochemical analyses, rock physics relationships, seismic inversion signatures, and the derived seismic facies. For both simplicity and consistency, our study focuses on two rock physics models. P-wave velocity and density data have approximate ranges of ~2.2–3.6 km/s and ~2.3–3.0 g/cm^3. Poisson's ratio and Young's modulus, calculated from these two basic parameters and S-wave velocity, have a range of ~0.2–0.4 and ~10–80 GPa. In an X–Y plot, Gardner and mudrock slopes (Gardner et al., 1974; Castagna et al., 1985), key inputs to the seismic inversion, are calculated utilizing rock physics modeling and are 0.3 and 0.86, respectively, for the organic-rich shale portion of the Draupne Formation. For Gardner slope estimation, the X–Y plot is density-Vp, and for mudrock estimation, the plot is Vs-Vp. Comparisons of the organic maturation product, as seismic facies, with the seismic inversion results is instructive because there is an effect of both TOC content and maturation on seismic inversion parameters, i.e., P-Impedance, S-Impedance, and Poisson's ratio.

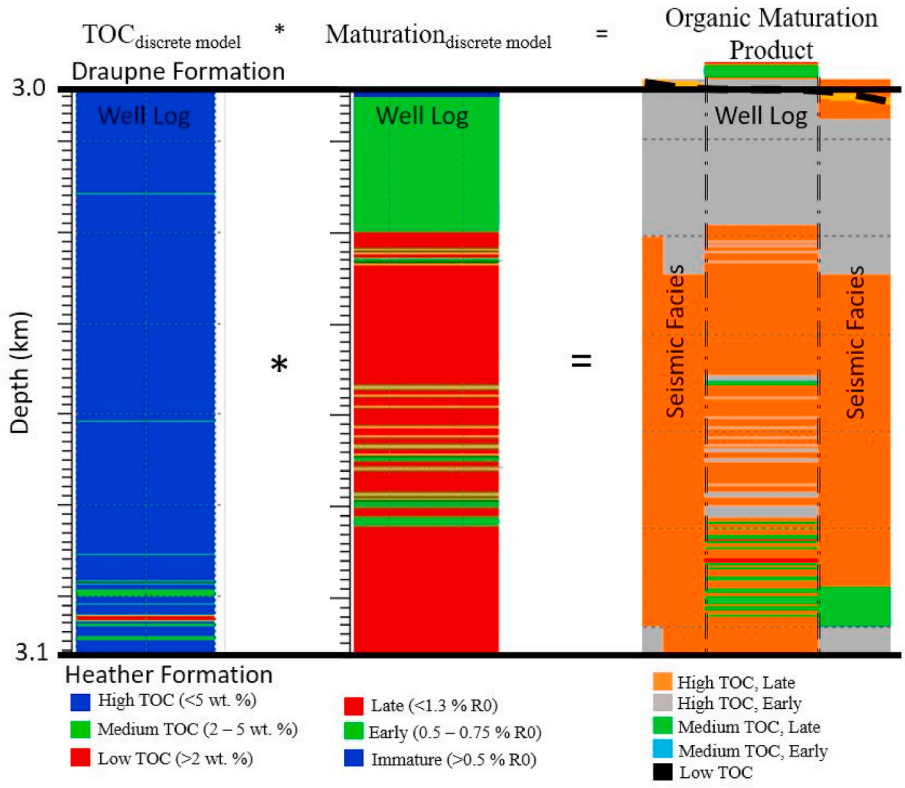

Fig. 5. TOC discrete model (left column) and maturation discrete model (middle column) for well 15/9–18, with the resulting Organic Maturation Product, OMP (right column). The corresponding seismic facies (3D seismic Survey B) is indicated for the well sitting on the background in the right column. TOC is separated out into low, medium, and high values. Maturation is separated out into immature, early oil generation, and late oil generation. A higher spatial resolution is present for the well log data than for the seismic data, and therefore more details are represented in the well log data. Considering the difference in spatial resolution, the background trend is consistent between the well log and the seismic data.

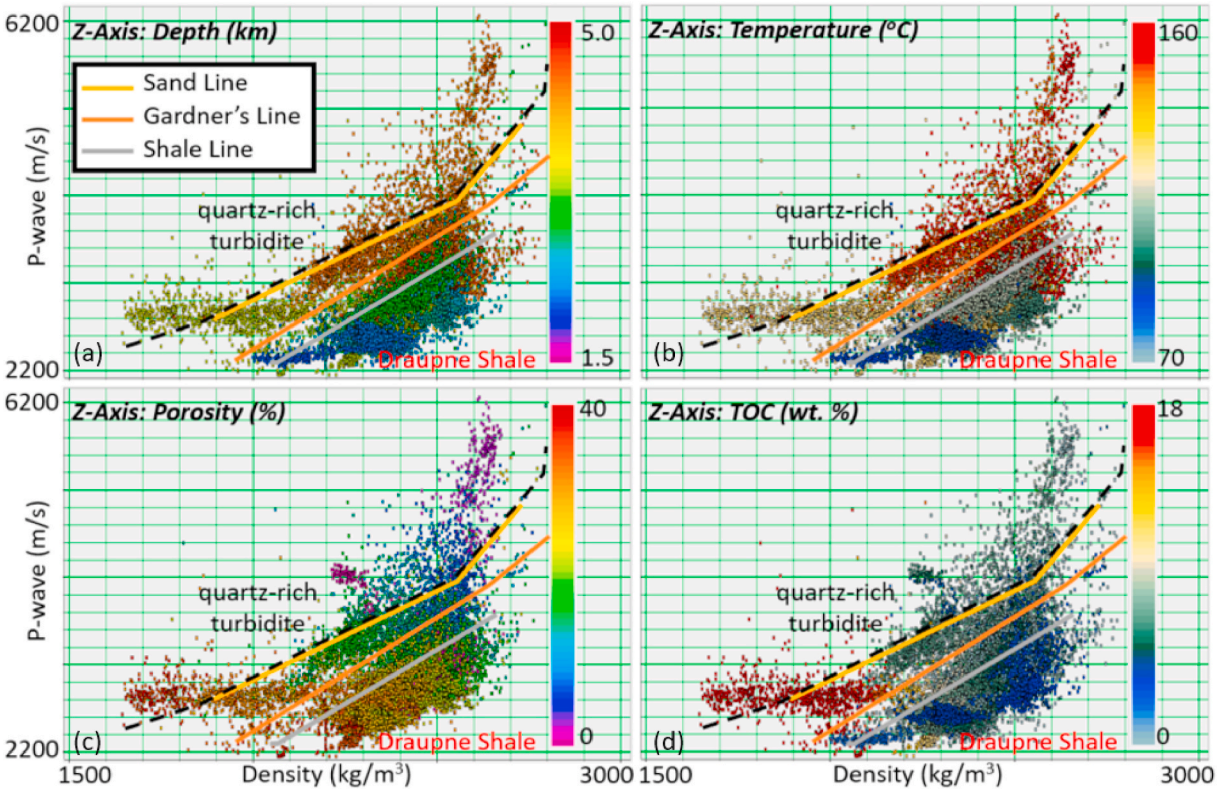

Fig. 6. Four parameters on a P-wave velocity versus density rock physics template. P-wave velocity and density in Draupne shale rocks are crossplotted with depth (a), temperature (b), porosity (c), and TOC (d). Averages for sand and shale facies are shown in yellow and grey, respectively, with Gardner's relationship in orange (Gardner et al., 1974). Data above the sand line (yellow) show quartz-rich intra-Draupne turbidites, while data below the shale line (grey) correspond to extremely clay-rich Draupne shale. Between these two lines, data contain shales with varying amounts of quartz content. In this study, data points located above the black dashed line are related to quartz-rich intra-Draupne turbidites, for which the TOC content values are meaningless in plot (d). (For interpretation of the references to color in this figure legend, the reader is referred to the Web version of this article.)

4.1. Rock physics analysis

A clear link exists between depth and elastic properties, wave velocities, and density (Fig. 6a). The increase in bulk density and V_p is likely due to compaction with depth. An inspection of the data utilizing the rock physics template proposed by Perez and Marfurt (2014) for geomechanical studies shows a relationship between depth and mechanical properties where shallower rocks are more ductile in nature than deeper rocks (Fig. 7a). However, data confirm that depth alone does not explain the mechanical properties of the rock (Fig. 7a). The Gardner relationship shows a separation between the organic-rich shale from the turbiditic quartz-rich sequences (Fig. 6). Averages for quartz-rich rocks and clay-rich rocks are located above and below the Gardner relationship, respectively. Any values for TOC above the sand line (Fig. 6d) must be strictly ignored as TOC is not present in the quartz-rich sequences. It can be seen that the average depths of the quartz-rich turbiditic sequences are typically deeper than that of the organic-rich shales. However, there are some shallow quartz-rich sections as well (Fig. 6a). Organic-rich shales make up a larger portion of this dataset, with more variable depths than the turbiditic sequences.

Similar to the increase in depth, a general rise in temperature relates to the increase in P-wave velocity and density (Fig. 6b). The clay-rich rocks in the data set cover a substantial range of temperatures from ~70 to 160 °C. These significant ranges of temperatures were seen for all the seismic wave velocities with high clay content (Fig. 6b). Overall temperatures tended to be higher for the turbidites than the organic-rich shale. While this effect may be partly attributed to quartz-rich rocks transmitting heat better than clay-rich rocks, as demonstrated experimentally by Robertson (1988), the dominant influence is likely the typical thermal trends with depth.

An inverse relationship exists between porosity and P-wave velocity (Fig. 6c), where shallower rocks tended to have higher porosity values. Porosity also tends to have an inverse correlation with both temperature and depth due to overriding compaction trends (Fig. 6c). However, the data show a smaller range of porosity for the clay-rich shale despite a larger range for both depth and temperature (Fig. 6c). Nonetheless, a deviation from this effect is clearly shown for the Draupne Formation over an extensive range of depths within a dataset (Fig. 7c). Both the highest and lowest porosity rocks are ductile, while a range between these can be classified as being increasingly brittle. A closer inspection of the dataset shows that the orientation of the porosity crosscuts the rock physics template describing the mechanical nature of the rock.

The relationship between TOC and seismic wave velocity properties is more complex, although trends are still present (Fig. 6d). Clear local variations are present within TOC compositions. This varied from all of the other trends, which are readily seen utilizing the Vp-density rock physics template (Fig. 6a–c). However, a comparison between depth and TOC for the Vp-density plots does reveal that higher values of TOC tend to be present for shallower portions of the Draupne Formation. This can also be seen on Young's modulus-Poisson's ratio crossplot (Fig. 7d). Isaksen and Ledje (2001) separated the Draupne formation into Upper and Lower sections, showing that the Upper section had a tendency to be more TOC-rich. This means that both regionally and locally, rocks tend to be more TOC-rich when shallower. The key to the more precise separation of TOC within the elastic parameters is the S-wave component present in both Poisson's ratio and Young's modulus (Fig. 7d), as shown by a comparison of the two rock physics templates.

The rock physics template used for geomechanical studies shows a porosity-dependent relationship between TOC and the mechanical behavior of the material. Specifically, there is a general trend wherein

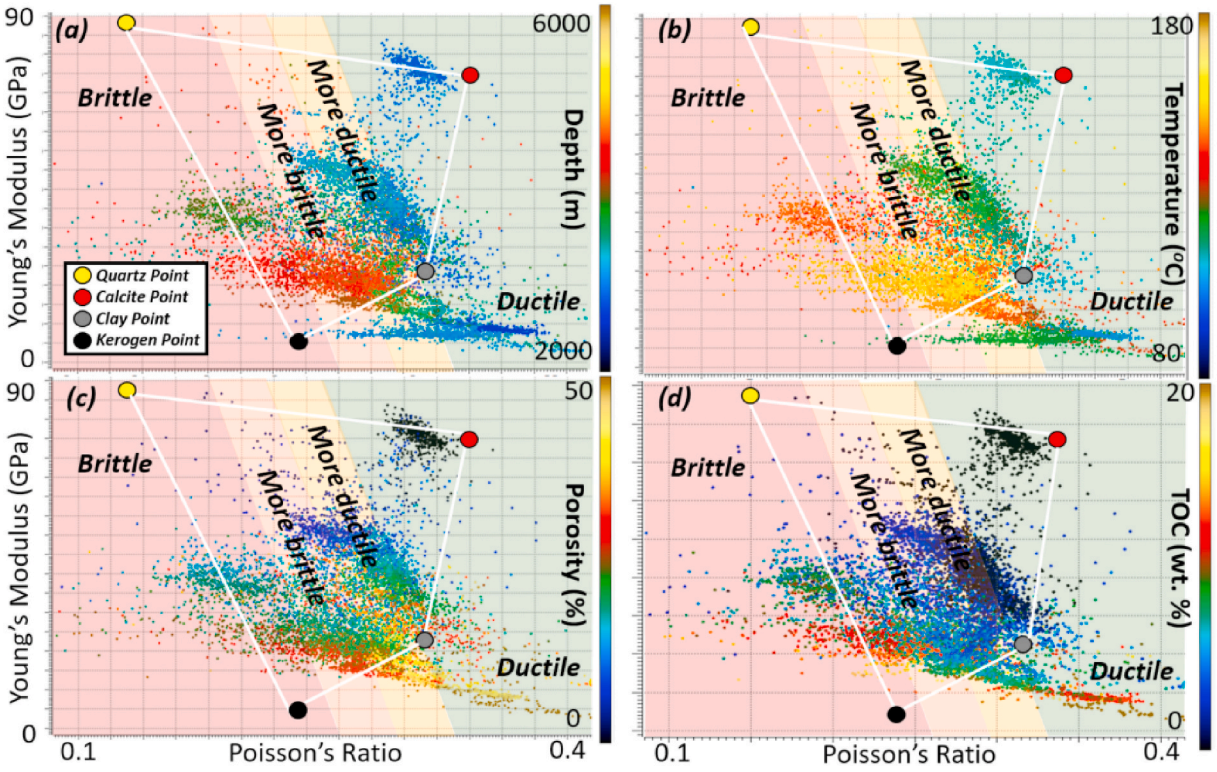

Fig. 7. Four parameters on Young's modulus versus Poisson's ratio rock physics template. Young's modulus and Poisson's ratio in Draupne shale rocks with depth (a), temperature (b), porosity (c), and TOC (d). The separation of the rock into regimes ranging from ductile to brittle (Perez and Marfurt, 2014) is overlain. Points representative of different materials (quartz, calcite, clay, kerogen) have also been overlaid (Mondol, 2018).

higher TOC correlates to more brittle behavior (Fig. 7d). However, TOC-rich shale can behave more ductile if it also has higher porosity (high values of ν, low values of E; Fig. 7c and d). Therefore, the relationship between TOC and its mechanical behavior is best considered with knowledge of porosity values.

Fig. 7b shows a generally positive trend between increasing

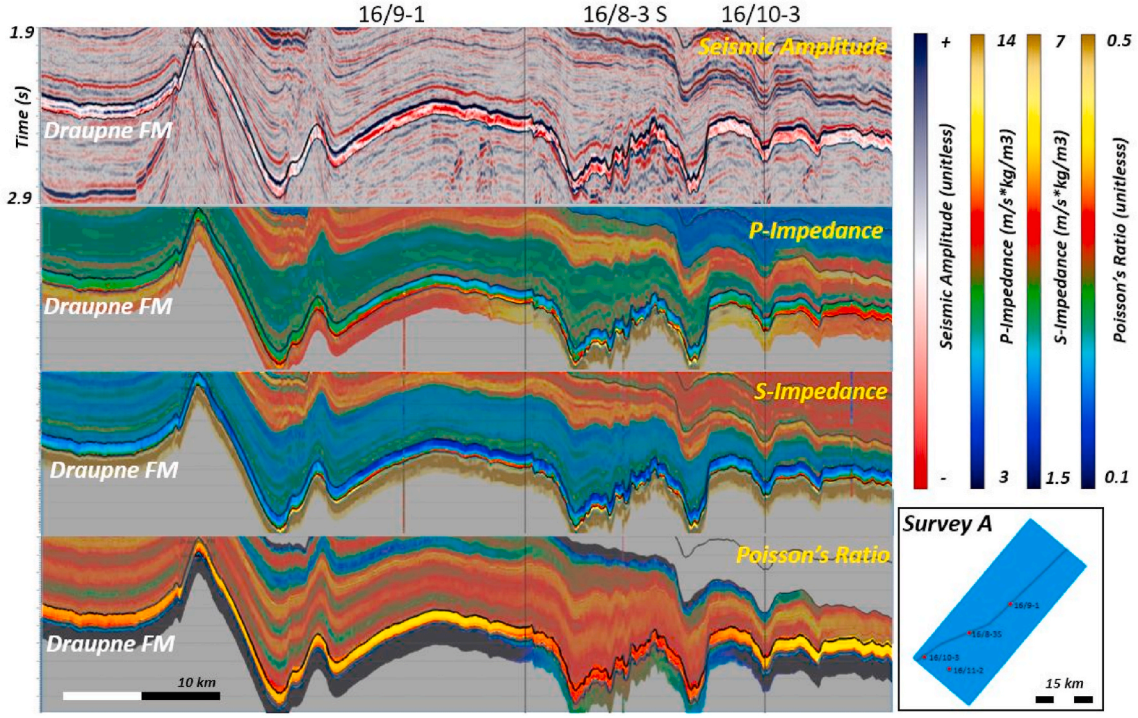

Fig. 8. Comparisons of seismic data with P-Impedance, S-Impedance, and Poisson's ratio with a focus on the Draupne Formation (layer with brighter colors), along a cross-section extracted from an arbitrary profile in Survey A shown in the bottom right inset. (For interpretation of the references to color in this figure legend, the reader is referred to the Web version of this article.)

temperature and brittleness, as expected, however here too, exceptions exist. Specifically, it can be noted that both depth and temperature trends show TOC-rich shale that is increasingly more brittle than their TOC-poor counterparts at similar depths and temperatures (Fig. 7a, b, and d). Finally, it should also be noted that salt intrusions have been shown to significantly alter the thermal gradient (Daniilidis and Herber, 2017) where present and that salt intrusions are clearly visible around Survey A (Fig. 8).

4.2. Mapping rock properties utilizing seismic inversion

Since our dataset includes two 3D seismic volumes, it is possible to map two distinct sections of the basin in terms of depth, temperature, and maturation. While a time-depth conversion of the seismic dataset is beyond the scope of this study, well logs place the Draupne Formation for Survey A at a range of depths of ~2000–2600m. Based on well log data, the depths of the Draupne Formation for Survey B have a range of ~3200–3800m. Rock physics templates show a positive correlation between depth and temperature suggesting ranges of ~82–101 °C and ~119–138 °C for Survey A and B, respectively. However, the temperature range can have a deviation as large as 25 °C higher due to salt intrusions from the background trend (Daniilidis and Herber, 2017). Seismic inversion results included the original amplitude volumes and the seismic inversion derivative volumes of P-Impedance, S-Impedance, and Poisson's ratio. While 3D volumes of Young's modulus can also be created, they were not included here as they rely upon having well-interpreted density results in addition to P-wave and S-wave velocity seismic data sets.

Within Survey A, the Draupne Formation generally appears to have one interface within the formation, as seen on the seismic data. Salt diapirs are present around the formation in two areas towards the shallower section of the arbitrary cross-section, as marked by the dashed outlines (Fig. 8). The P-Impedance and S-Impedance seismic datasets revealed that the Draupne Formation could be classified into upper and lower layers, where the lower layer has significantly higher impedance values. While the Draupne Formation has lower impedance values than both the overlying Åsgard Formation and the underlying Vestland Group, the transition is sharper with the latter. The difference between impedance values is consistent with lithological variations, confirmed by both core and well log analysis. However, the variation in impedance values internal to the Draupne Formation cannot be lithological or mineralogical, as Hansen et al. (2020) showed that disparate data geographically within our study area share the same portion of a mineralogical ternary diagram. Poisson's ratio could not separate the two layers; however, it shows where the Draupne Formation stands mechanically different from the surrounding layers.

For Survey B, the 3D seismic dataset indicates two clear interfaces for the Draupne Formation. Both P-Impedance and S-Impedance results reveal a more complex picture than for Survey A (Fig. 9). The impedance volumes extracted show that the Draupne Formation separates into three layers instead of the expected two layers in this part of the basin. The bottom and top layers typically have lower values of impedance than the central layer, whose values best mimic the overlying Åsgard Formation or underlying Heather or Hugin Formations. While it is known that the impedance differences between formations are lithological, the extreme contrast between values could be indicative of a lithological difference due to the intra-Draupne turbiditic sands. Both well log analysis and core photos available support the interpretation that the central layer is a quartz-rich turbiditic sequence for some of those wells in Survey B. Interestingly, within the Draupne Formation, the impedance trends for Survey B are opposite of those for Survey A. The higher impedance values are in the upper Draupne Formation, as opposed to the lower Draupne Formation. It was difficult to separate the Poisson's ratio into different sub-layers of the Draupne Formation, likely due to similarly low values for both the P-Impedance and S-Impedance data. A comparison of the two 3D seismic datasets revealed that while impedance data have similar values, there is a marked change in the Poisson's ratio with a decrease from Survey A to Survey B (Figs. 8 and 9). Based on established rock physics trends, this would indicate that the deeper Survey B is generally more brittle.

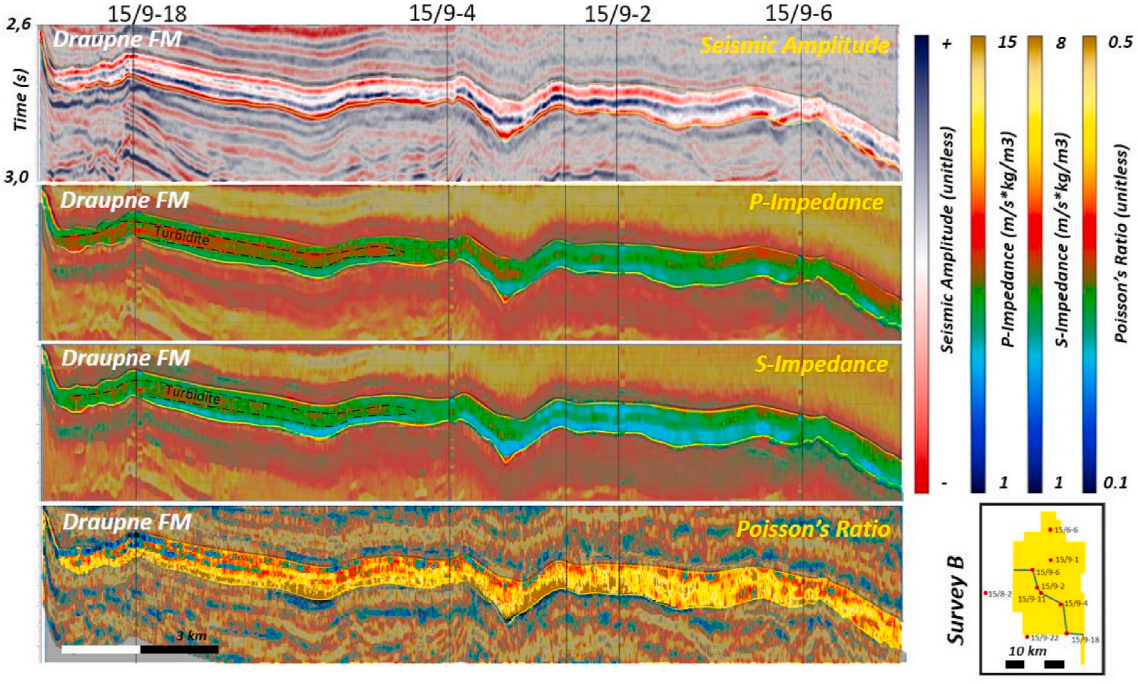

Fig. 9. Comparisons of seismic with P-Impedance, S-Impedance, and Poisson's ratio with a focus on the Draupne Formation (layer with brighter colors), along a cross-section extracted from an arbitrary line in Survey B. Interlayered turbidite highlighted by significantly different impedance values are outlined with a black dashed line in the P-Impedance and S-Impedance panels. (For interpretation of the references to color in this figure legend, the reader is referred to the Web version of this article.)

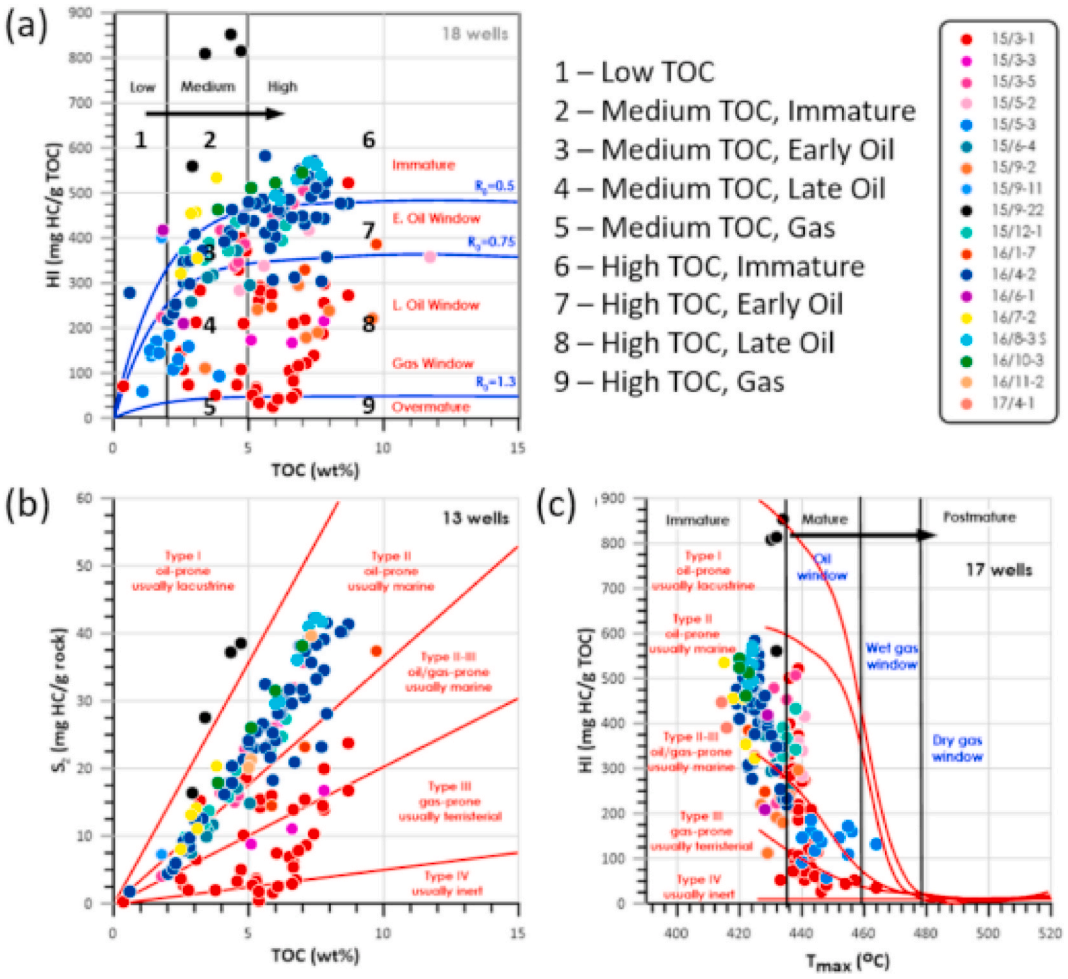

Fig. 10. (a) Hydrogen Index (HI) versus TOC (wt. %) plot from the wells in our dataset allows estimating vitrinite reflectance values (modified from Vernik and Landis, 1996). (b) S2 vs. TOC (wt. %) shows kerogen type and its likely origin, and (c) Hydrogen Index versus T_{max} shows both kerogen type and a general maturation trend (modified from Isaksen and Ledje, 2001).

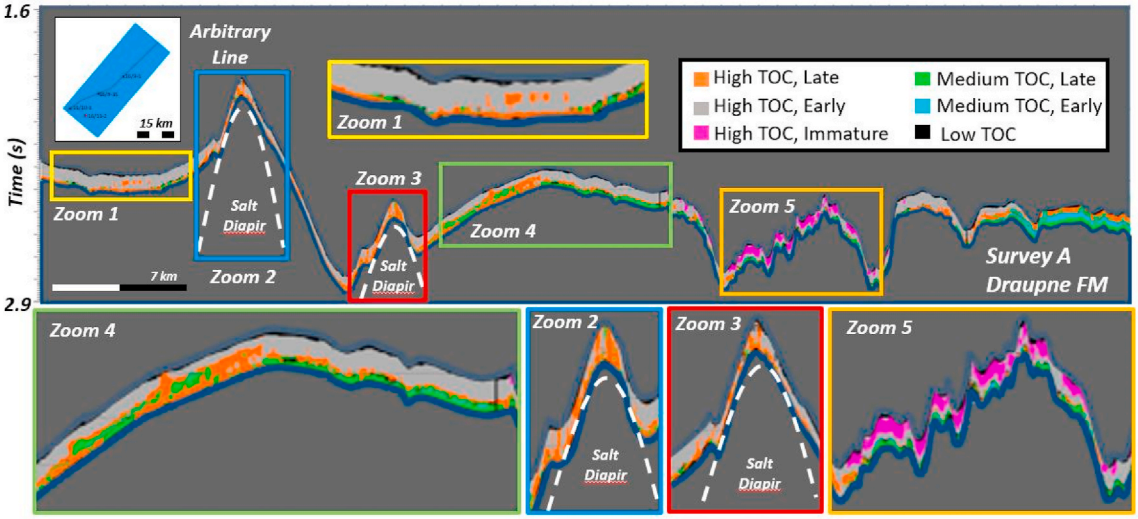

Fig. 11. Values of the organic maturation product (OMP) for the Draupne Formation in a cross-section extracted in Survey A along an arbitrary profile (black line in the upper left inset). Zoomed in sections show details. The impact of maturation on shale due to a salt diapir's proximity is observed (zooms 2 and 3), while zooms 4 and 5 better show stratigraphical separations of maturation.

4.3. Interplay between organic content and maturation

Maturation, TOC content, and kerogen type are the main results from the laboratory geochemical analyses. Kerogen type is predominantly Type II, Type II-III, and Type III with some Type I and Type IV (Fig. 10b). TOC content within the study area is known to vary from 0 to 20 wt % (Thyberg et al., 2010; Zadeh et al., 2017). However, the geochemical data show a more constricted range from 0 to 12 wt % (Fig. 10a and b), with data below ~2 wt % not always being included in the geochemical reports. Rock physics templates show that well log data have a similar TOC range with the highest values around 15 wt% (Figs. 6d and 7d). Understanding maturation, utilizing vitrinite reflectance or an estimate thereof as a proxy, is the main outcome from the geochemical analysis. The dataset is shown to range from immature to late oil generation and possibly into the gas generation window (Fig. 10a and c). However, the majority of data points are located within the immature to oil generation window. Geochemical data indicate that wells around Survey A are predominantly drilled in the immature to early oil generation window, with some in the late oil generation window. In contrast, wells around Survey B are primarily drilled in the early oil generation to late oil generation windows, with some in the early gas window (Fig. 10a and c). Fig. 10a displays how the Organic Maturation Product (OMP) maps can be compared with Vernik and Landis (1996) HI versus TOC cross-plot. Based on the geochemical data, TOC ranges are similar for Surveys A and B.

4.4. Mapping of the organic maturation product (OMP)

Distribution of the seismic facies and of the proposed Organic Maturation Product (OMP), both for the wells and the seismic datasets, confirm that higher TOC is more predominant in the upper Draupne Formation, while medium and low TOC values can more often be found in the lower Draupne Formation (Figs. 11 and 12). In terms of estimated vitrinite reflectance, Survey A is primarily immature or within the early oil generation window, with a few areas showing late oil generation. The areas that show late oil generation are located nearby salt intrusions. The organic maturation product (OMP), which depends on both TOC and vitrinite reflectance along an arbitrary cross-section into the 3D seismic dataset generally increasing in-depth, shows that TOC progresses typically from high to medium, with occasional patches of lower TOC (Fig. 11, zooms 4 and 5). Likewise, maturation progresses with depth unless special conditions, like salt diapirs that alter the temperature trend locally (zooms 2 and 3, Fig. 11). Note that the arbitrary profiles were chosen to best represent data while coinciding with the well logs. Since organic-rich shale is the focus of the present study, these profiles were chosen to illustrate key aspects of our study (Figs. 11 and 12).

However, in contrast to Survey A, the patches of medium TOC in Survey B are more localized, with higher TOC regions being more pervasive (zoom 2, Fig. 12). Since Survey B is also the deepest dataset within a relatively simplistic depositional basin, this deeper location explains why more shale is situated within the late oil generation window. However, some of the shales of Survey B remained within the early oil generation window (zoom 3, Fig. 12). There was little to no presence of immature organic-rich shale in this dataset. Along an arbitrary profile generally increasing with depth, a pattern common to this dataset is visible: organic-rich shale of a given maturity has a window of another maturity encompassing it (e.g., zoom 2, Fig. 12). However, in some sections maturation breaks through vertically, possibly identifying zones of greater thermal maturity (zoom 3, Fig. 12). Note, zones shown to be turbidite in Fig. 9, can be discounted in Fig. 12 (zoom 1) as they represent the quartz-rich turbidite section.

Fig. 13 displays stratigraphic slices of the Organic Maturation Product at two different depths for each Survey. Fig. 13a shows lateral variations in TOC content. Fig. 13b mainly shows the contrast in maturation, while the TOC content remained largely the same throughout. The exception to this is a section of medium TOC with variable maturation in the southwest corner of Survey A (Fig. 13b). A comparison of Figs. 11 and 13a revealed some similarities between the structure of the Draupne Formation and the distribution of maturation. Notably, the comparison of figures showed a generally positive spatial correlation between maturation and depth, with some notable exceptions due to the effect of salt intrusions, as discussed later. Deeper within Survey A, a contrast in TOC content is present (Fig. 13b). While there was no clear relationship between structure and the contrast in TOC content, the organic maturation product (OMP) based on seismic reflectivity may indicate a pattern similar to that found in alluvial depositional systems. In alluvial systems, some channel-like structures of high TOC are surrounded by bank-like structures of medium TOC (Fig. 13a). An investigation of Survey B (Fig. 13c and d) indicates that the shallower stratal slice (Fig. 13c) and the deeper stratal slice (Fig. 13d) show a less distinguishable geomorphological shape when comparing TOC content that could be related to fan structures. The comparison between structure and maturation for Survey B shows a

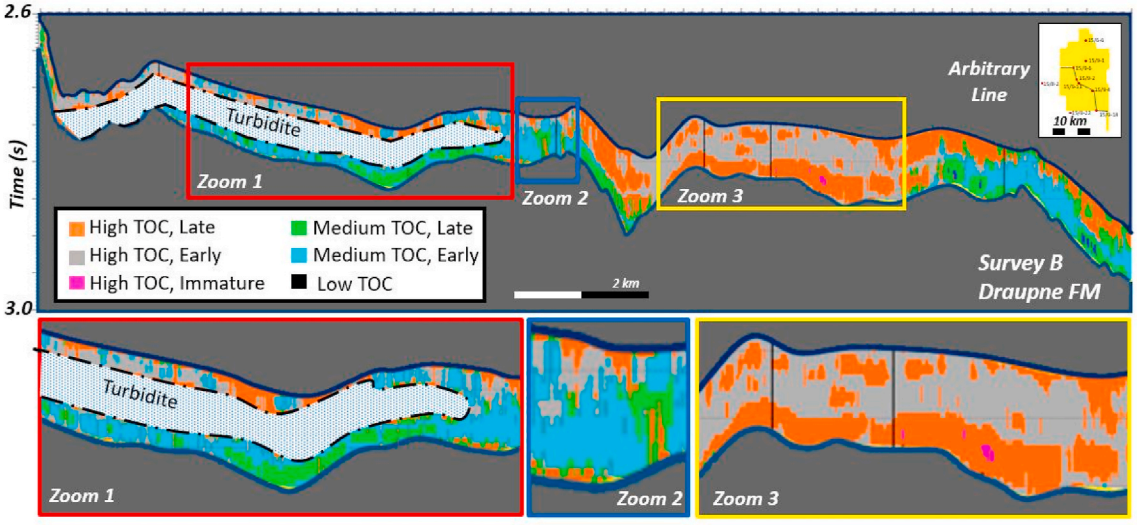

Fig. 12. Values for the organic maturation product (OMP) for the Draupne Formation in a cross-section extracted in Survey B along an arbitrary profile (black line in the upper right inset). The turbidite section, observed from the seismic inversion results and the P-Impedance and S-Impedance, is outlined in dashed black and marked. As such, the OMP results in the turbidite do not represent anything real since no TOC can exist for a quartz-rich turbidite.

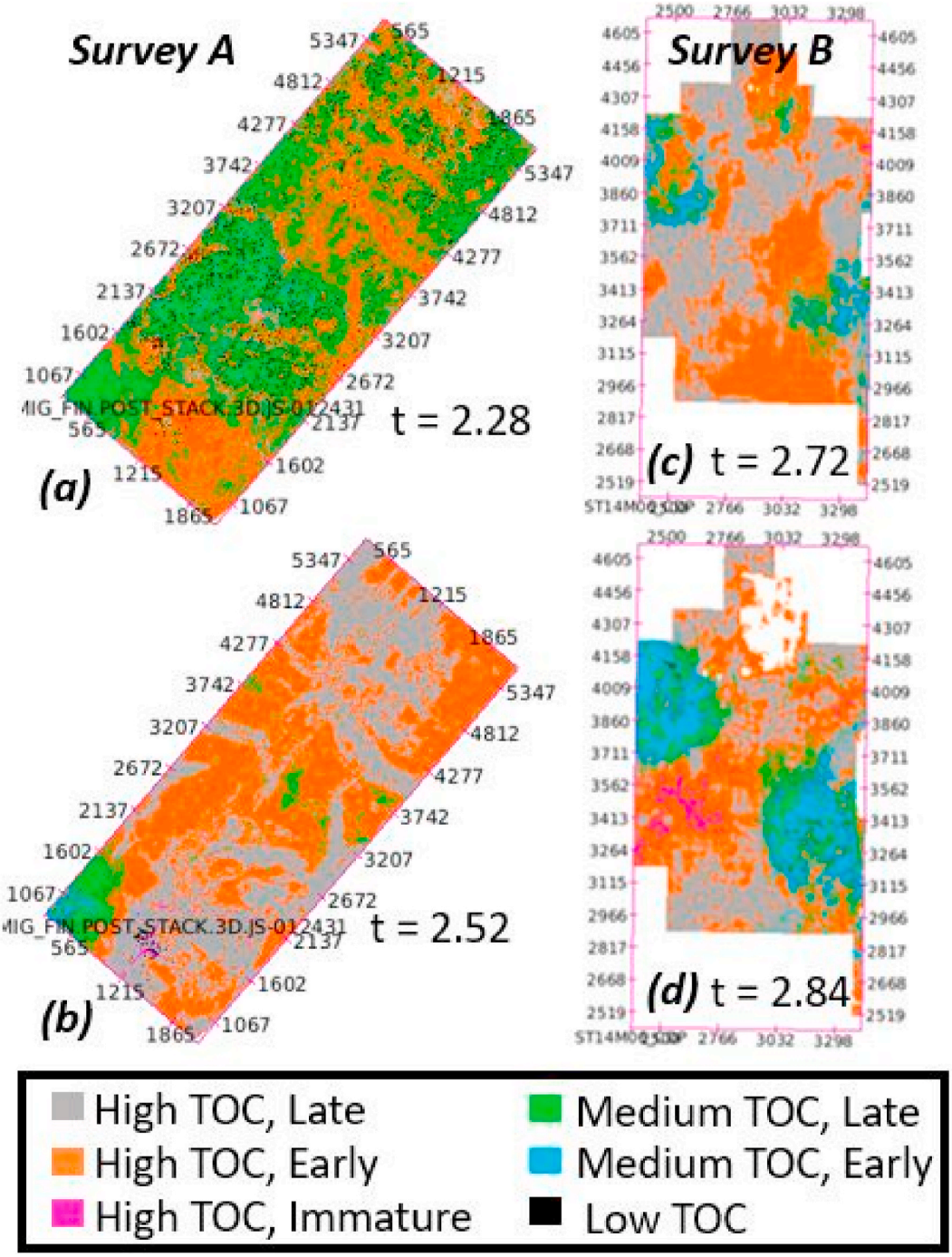

Fig. 13. Map view of stratal slices of the organic maturation product at two different depths for Survey A (a, b) and Survey B (c, d).

positive correlation between depth and maturation. An internal pattern for maturation is present, showing fan-like structures that are particularly apparent for the medium TOC data in Fig. 13d.

The presence of salt diapirism within the study area may modify the relationship between TOC, maturation, and brittleness. We performed a comparison between the frequency of different organic maturation products (OMPs) for the entire Survey A (Fig. 14b), and for a small subset volume focused around a single salt diaper (Fig. 14a). The salt diapir can be seen on both cross-section and map view due to its direct effect on the structure within the area (Figs. 8, 14c and 14d). For the diapir dataset, the two highest groups are Late Oil Generation, either Medium or High TOC. The next largest groups in terms of frequency is Early Oil Generation, either Medium or High TOC. Immature products for both Medium and High TOC have the lowest frequency alongside Low TOC (Fig. 14a). The results for Survey A differed from those seen for the salt diapir dataset, wherein the two categories with the highest frequencies are Medium TOC, with either Late Oil Generation or Early Oil Generation. This is followed by an almost equally high frequency of High TOC, Late Oil Generation. After that, significantly lower levels can be seen for High TOC and Early Oil Generation. While the results for immature shale were roughly the same for the salt diapir and Survey A, there is a marked difference for Low TOC. Significantly higher values for Low TOC are present in Survey A as a whole (Fig. 14b) than for the salt diapir sub-volume (Fig. 14a).

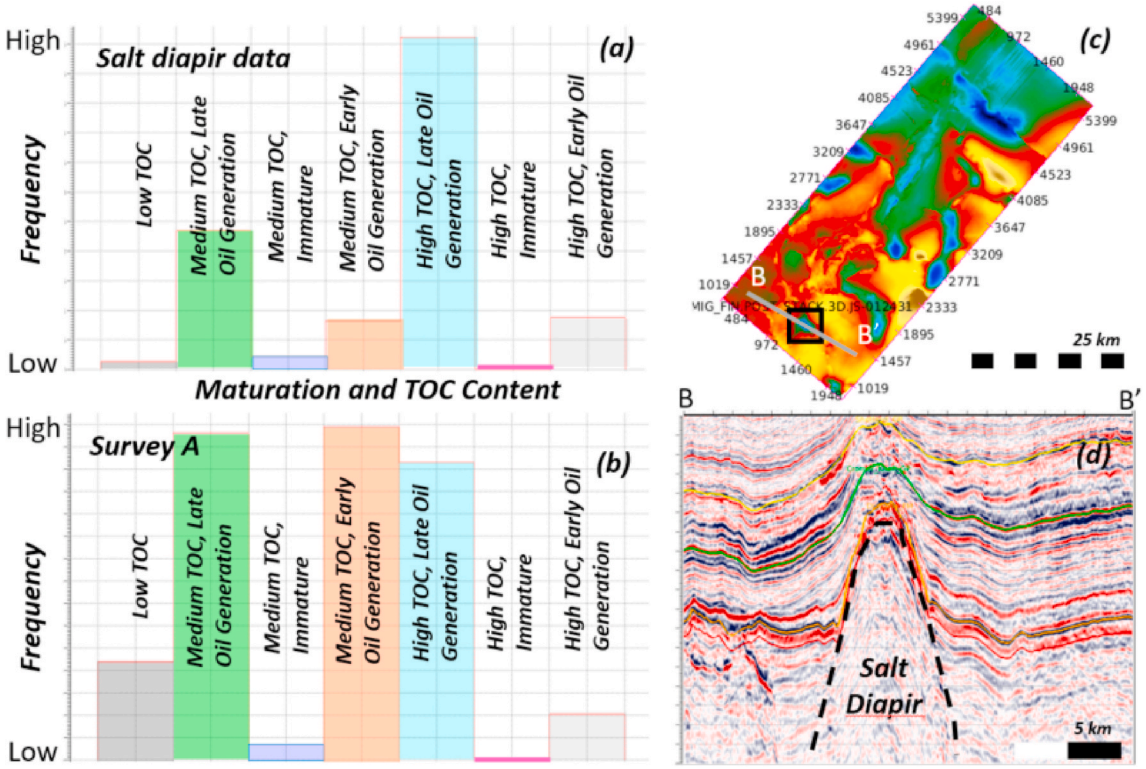

Fig. 14. Distribution of maturation and TOC content, with the frequency of those around a salt diapir (a) and for the entire Survey A (b). The line B–B′ in panel (c) shows the salt diapir displayed in (d).

5. Discussion

The distribution of organic matter, both in terms of the percentage of the rock it constitutes and its geographical location, is critical to understanding the quality of source rocks (Sonnenberg and Meckel, 2017). As a result, understanding the relationship between TOC and organic matter maturation directly impacts drilling success for both conventional and unconventional hydrocarbon resources. High TOC alone does not control the quality of source rock. The degree of maturation the kerogen has undergone dictates the total amount of hydrocarbon produced (Tissot and Welte, 1984; Welte et al., 1997; Ward, 2010). Maturation also has a significant impact on the caprock shales' mechanical properties during and after the conversion of kerogen into hydrocarbon (Prasad et al., 2011; Anders et al., 2014; Zargari et al., 2016; Craddock et al., 2018). The interplay between TOC and maturation as it applies to an organic-rich shale's brittleness allows one to better understand both parameters as they interact with one another and organic-rich shale as a whole. Mapping the organic maturation product (OMP), utilizing seismic inversion and derived seismic facies provides an opportunity to understand what role deposition played in the distribution of kerogen and how diagenetic trends impacted the maturation of kerogen.

5.1. Mapping of TOC and maturation (OMP) - depositional trends

The sediments of the Draupne Formation can be classified into two categories, (1) deep marine anoxic deposits, separated by (2) turbidites or debris-flows (Bugge et al., 2001; Isaksen and Ledje, 2001; Olsen et al., 2017). Even if a depositional system is deep, marine, and anoxic in nature, water bottom currents may occur(Arthur and Sageman, 1994). Literature in comparable portions of the Norwegian North Sea shows that the kerogen type is predominantly Type II and Type III in the North Sea (Isaksen and Ledje, 2001; Hansen et al., 2019). Deep marine anoxic deposition of the organic-rich shale is characterized by relatively low P-Impedance and S-Impedance. P-impedance is high for the intra-Draupne turbiditic flows, while the V_p/V_s is comparably lower (data points above the sand line in Figs. 6 and 9). This is a lithologic indicator as shales usually have higher V_p/V_s values with lower P-Impedance than sand-rich turbiditic deposits (Pendrel et al., 1999; Avseth et al., 2001; Inichinbia et al., 2014), and falls in line with literature on turbidites in the study area (Olsen et al., 2017). Well logs and core data further confirm the presence of turbidites in this area.

Not only can the Draupne Formation be separated into two key lithologies, where the focus of this study is on the organic-rich shale, but it can also be separated into the Upper and Lower Draupne Formation, as proposed by Isaksen and Ledje (2001). This separation is defined by a contrast in the amount of TOC regionally (Isaksen and Ledje, 2001), as well as within our study area (Løseth et al., 2011; Hansen et al., 2020; present study). This increase in TOC towards the Upper Draupne Formation becomes very clear when one looks at the rock physics data and comparing depth with TOC (Fig. 6a, d,7a, 7d). Survey A shows higher impedance values associated with the Lower Draupne Formation (Fig. 8). Since the Upper and Lower Draupne Formations are similar in terms of both lithology and mineralogy (Hansen et al., 2020), excluding the presence of turbidites, one can conclude that this difference is likely the result of TOC. Løseth et al. (2011) noted that it is both possible to separate hydrocarbon source rocks on seismic data, and, as confirmed by other studies, all other things being equal, an increase in impedance results in a decrease in TOC (Broadhead, 2016; Hansen et al., 2019).

Further to this, Hansen et al. (2020) proposed to model the impact of TOC on the Draupne Formation on our study area. Utilizing the approach of Vernik (2016), these authors noted that an increase in TOC from 1.5 wt% to 6.5 wt% would result in a decrease of P-wave velocity by 0.6 km/s and a decrease of 0.15 g/cm^3 for density. Note that the similarity in mineralogy is also partially confirmed by the material points (circles in Fig. 7), based on Mondol (2018). The organic-rich shale portion of the Draupne Formation is shown to plot entirely between the clay and kerogen material points, with a slight skew towards quartz (Fig. 7). It is only in the very low TOC data that it skews towards the

calcite point; however, this is likely due to other factors, as calcareous cement is not common in the Draupne Formation (NPD, 2021).

At the macro-scale, the nature of depositional features varies between Survey A and Survey B. Specifically, submarine channels consisting entirely of fine-grain sediment (i.e., shale, either organic-rich or not) are present within Survey A (Fig. 13a and b). In contrast, submarine fan features are visible on the pre-stack volume of Survey B (Fig. 13c and d). These features fall in-line with their historical proximity to the shoreline and the depositional nature of debris flows (Reading and Richards, 1994; Stow and Mayall, 2000; Olsen et al., 2017). Note the features we see here are composed of the organic-rich shale as indicated by the impedance values and the well log and core data. Depending on the stratal slice, these different depositional features are clearly present (Fig. 13). Medium TOC floodbank-like deposits (Fig. 13a) surround high TOC channel-like structures. Since kerogen is a major constituent of the Draupne Formation, i.e., up to 20 wt% (Løseth et al., 2011), it is conceivable that TOC would interact with deposition as indicated by the stratal slices. Additionally, if TOC data were to interact with deposition, the lower density range of kerogen compared to the other constituents of shales would indicate that TOC would ultimately be higher in rocks formed from the lowest velocity settings deposition.

The shape of fans (Reading and Richards, 1994; Stow and Mayall, 2000) and the shape of wind transported sediment deposits (Blakey and Middleton, 1983) can bear a resemblance to one another. All shapes are seen in Fig. 13b, c, and 13d represent either the front of a fan or pelagic deposition. Kerogen density may assist in higher TOC sediments moving farther than medium TOC sediments, allowing high TOC sediments to sit outside the rim or on the 'over banks' of the medium TOC sediments. In contrast to this, wind-blown deposition is near structureless, allowing an intermixed set of medium and high TOC layers without clear patterns. Fig. 13d better represents an alluvial fan terminus with this additional data, while Fig. 13b and c could better represent wind-blown deposition. Regardless, the data indicates that TOC content impacts depositional features that can be separated in seismic facies within fine-grain sediments (i.e., shale, organic-rich, or not).

5.2. Mapping of TOC and maturation (OMP) – diagenetic trends

Diagenesis of shale directly impacts its capacity to be a seal (Katsube and Williamson, 1994) and controls the hydrocarbon potential of source rocks (Tissot and Welte, 1984). Another impact of increasing temperature and pressure, alongside with depth, is the creation of salt intrusions from previously salt-rich layers (Antoine and Bryant, 1969). Comparing the two 3D seismic datasets shows another impact of variable levels of diagenesis, specifically on the seismic wave parameters and their elastic derivatives. A reduction in Poisson's ratio from Survey A to B, utilizing the rock physics model from Perez and Marfurt (2014), would indicate a movement towards increased brittleness. This is consistent with what one should expect for seismic surveys taken from different depths.

While TOC distribution can be linked to depositional patterns, maturation occurs as a part of diagenesis (Anders et al., 2014). As part of this study, we confirmed that a correlation exists between depth and maturation in this part of the North Sea. This correlation is primarily due to the relatively simple diagenetic history, wherein rifting in the Late Jurassic resulted in the deposition of the Draupne Formation that was subsequently buried relatively continuously without significant uplift afterward (Bugge et al., 2001; Hansen et al., 2020). Furthermore, a comparison of the maturity results from Fig. 4 with the estimations of vitrinite reflectance as a proxy for maturity in Fig. 10, due to the limited amount of vitrinite reflectance data, confirms that the work from Vernik and Landis (1996) also applies to our data set. Additionally, a general comparison of maturation windows with the data from wells around Surveys A and B show that the different approaches produce comparable results.

However, the amount of shale compaction decreases with depth in our data, which is consistent with the literature (Magara, 1980; Dutta et al., 2009), while the compaction for the quartz-rich rock remains relatively constant with depth (Fig. 6a and c). It has long been established that shale's compaction trends are more complicated than they are for sandstone (Magara, 1980; Baldwin and Butler, 1985; Mondol et al., 2007). A possible explanation for the inconsistency with the literature is that the maturation of organic matter can increase porosity (Yenugu and Han, 2013). It has been established that shale will undergo greater compaction, and therefore greater porosity changes than quartz-rich rocks will (Magara, 1980; Baldwin and Butler, 1985). However, deviations from this trend can be seen (Fig. 6) and can be partially explained by the diagenetic process. Prasad et al. (2009) noted that immature shales with a higher organic content will show an increase in P-wave velocity with burial depth, while shales that have undergone greater maturation will show the opposite effect. This is explained by the dual nature of kerogen, in that it will act as load-bearing until maturation occurs and then will become a part of the matrix leaving the clays as load-bearing (Prasad et al., 2009). One can also characterize how diagenesis affected the distribution of variably matured organic-rich shales (Figs. 11–13).

Salt diapirs have been shown to affect maturation, as the thermal conductivity in halite is significantly higher than in other lithologies (Jensen, 1983, 1990; Magri et al., 2008). As such, greater maturation should be present adjacent to the salt diapirs, as shown in both map view (Fig. 13a) and cross-sections (Figs. 8 and 11b) in the data of Survey A (Fig. 14b). Additionally, data show that the increased maturation's effect extends up to 150% of the salt intrusion radius size. This can then be compared to a more quantitative approach. The average distributions of maturation around the salt intrusions are compared to the background maturation in the 3D seismic dataset (Fig. 14). Results show an increase in maturation around the salt intrusions that deviates from the general trend between maturation and depth. This result indicates that salt diapirism influences the maturation of the Draupne Shale within the North Sea and confirms other studies (Jensen, 1983, 1990; Magri et al., 2008).

Since no salt intrusion could be detected in Survey B, this dataset cannot be used to further confirm the effect of diapirism on maturation. However, the lack of diapirism provided an opportunity to characterize factors that might control a deviation from the general trend between depth and maturation. A qualitative comparison of maturation with depth was carried out. Results show that maturation generally follows the geological structures in both map views (Fig. 11c and d) and cross-sections (Figs. 9 and 12).

Given the consistent difference in the amount of TOC for the Upper Draupne Formation compared to the Lower Draupne Formation, one can assume there was a significant dropoff in biological material being fed to the system during sedimentation. In our study, this difference can be used to show how differences in TOC and maturation interplay with one another to influence elastic parameters. Hansen et al. (2020) establish that lower TOC should increase both density and seismic wave velocity based on the work by Vernik (2016). As noted earlier, this is precisely what one sees for the impedance values for the shallower Survey A (Fig. 8), where the majority of shale exists in the immature to early oil generation window (Fig. 11). However, it is also established that increased maturity will have a dampening effect on both velocity and elastic parameters (Prasad et al., 2011; Zargari et al., 2016). Significantly deeper in the basin, at Survey B, the difference between the Upper and Lower Draupne Formations for impedance values is much closer, with the Lower Draupne Formation being slightly lower on average (Fig. 9). At this point, the Lower Draupne Formation is mostly in the late oil generation window (Fig. 12), while the Upper Draupne Formation is still in the early oil generation window (Fig. 12). These results are consistent with the study of Prasad et al. (2009), who suggested that kerogen's transformative effect on elastic properties has taken place, closing the difference between impedance values for Survey B.

5.3. Interplay between TOC and maturation (OMP) within a rock physics model

Many factors influence brittleness (i.e. mineralogy, pore pressure, fluid effects, etc.). Jarvie et al. (2007), Jin et al. (2014), and Alzahabi et al. (2015), highlight the importance of mineralogy, while other studies illustrate how stiff minerals can emplace themselves post-deposition (Thyberg et al., 2009; Avseth and Carcione, 2015). The process of maturation converts kerogen lenses into hydrocarbons, resulting in fluid expulsion and the creation of microfractures (Chauve et al., 2020). The impact that the fluids have on pore pressure is regulated by the interaction between the fluids and formation, particularly controlled by rate of absorption or fluid migration into surrounding formations (Rickman et al., 2008; Wu et al., 2016). While many studies have addressed the impacts of mineralogy, pore pressure, and fluid effects on brittleness (Table 4), fewer studies focus on the impact of TOC and maturation. The present study attempts to fill this gap by addressing the potential effects of TOC, and how maturation alters this impact.

Two interpretations have been proposed in the literature concerning the effect of TOC on the mechanical properties of organic-rich shales (Grieser and Bray, 2007; Wilson et al., 2017; Mondol, 2018), and is summarized in Table 4. The first interpretation correlates an increase in kerogen with an increase in brittleness, citing the presence of kerogen as a brittle constituent (Mondol, 2018). However, it is noted that pure clay content within organic-rich shale is more ductile in nature. These two interpretations provide two opposing trends within clays, one pulling it towards brittleness with the other pulling it towards a more ductile regime (Mondol, 2018). The second interpretation, proposed in a series of studies concerning shales in North and South America, has shown that higher values of TOC correlate to more ductile behavior (Grieser and Bray, 2007; Wilson et al., 2017). These studies had a particular interest in the content of kerogen as organic-rich shales provide an ideal reservoir when hydraulically fractured. However, a medium that is too ductile in nature will dampen the effect of artificial fracturing, and relatively quick healing of the fractures will occur, reducing permeability. Our study shows that an increase in TOC results in greater brittleness in our dataset (Fig. 15). The maturation of the kerogen within organic-rich shale could explain this disparity in the literature. By modeling vitrinite reflectance as a proxy for maturation, our data demonstrate the relationship between maturity and shale's mechanical properties is more complicated than shown by previous studies (Fig. 15).

Data from the two 3D seismic volumes (Fig. 15) clearly show a gradation from the brittle regime into the ductile through a comparison of TOC content alone. Low TOC rocks tend to populate the ductile regime in both datasets. Further to this observation, both medium and high TOC rocks grade into more brittle regimes based on maturation. Disparities exist in the number of data points available in the different 3D seismic datasets since they represent different depths and represent different levels of potential maturation. The frequency of higher elastic properties due to an increase in depth, especially with a higher level of TOC, is consistent with the literature (Zargari et al., 2013). Survey B contains more data points within the late oil generation window. From a comparison with Survey A, some trends emerge for the maturation as well.

Nonetheless, maturation increases as the organic-rich shale transition its mechanical state from ductile towards brittle. This process occurs at a faster rate for high TOC shale than for the same rock with medium TOC. High TOC, immature shale exists in the ductile regime, with early oil generation data dominantly plotting in a more ductile regime and with late oil generation data dominantly plotting in the more brittle regimes (Fig. 15). However, the relationship of the trend towards maturation depends on TOC. Note that for organic-rich shale with medium TOC, the trend is entirely different. Shales that are both immature and in early oil generation plot dominantly in the ductile regime (Fig. 15). However, medium TOC shale that has entered late oil generation plots predominantly in the more ductile regime and into the more brittle regime showing a marked increase in brittleness. Zargari et al. (2016) also studied this interaction, showing that Young's modulus of kerogen decreases when the kerogen is matured artificially in laboratory experiments. They account for this change as an impact of both increased porosity in remaining kerogen and the presence of fluids or gas with kerogen. This result could help account for why Young's modulus increases at a slower rate with higher TOC levels (Fig. 15). Another critical factor to consider is the changing nature of kerogen within the matrix as maturation occurs. Within immature organic-rich shales, kerogen is load-bearing, while it tends to become a part of the matrix leaving the grains as load-bearing in more mature shale (Prasad et al., 2009). This effect will correlate with the lower value of Poisson's ratio since higher P-wave velocity values relate to increased maturity (Fig. 15).

While no data points are available in our dataset within the gas generation window, one may extrapolate where these data would plot by extending the data available from both medium and high TOC. However, the influence of gas may have a notably stronger impact (Zargari et al., 2016). Note that while low TOC rock was not divided into possible maturation levels due to low kerogen content, the spread of data points, especially in Fig. 15a, indicates that maturation directly influences the shale's geomechanical properties even below a threshold of 2 wt% TOC.

Utilizing our dataset, we developed a rock physics template that classifies qualitatively the broad geomechanical trends for organic-rich shale at variable levels of TOC and maturation in the Draupne Formation (Fig. 16). Young's modulus more aptly separates variations in total TOC content than Poisson's ratio. As highlighted by Fig. 8, TOC better

Table 4
Studies on brittleness highlighting method used (elastic or mineralogy), study focus (brittleness), and any comments the study makes on TOC content and maturation.

Study	Brittleness Method Utilized	Paper Focus (Brittleness)	Comments from study on influence of TOC and maturation
Jarvie et al. (2007)	Mineralogy	Mineralogy dominates, TOC is not considered	Not considered
Jin et al. (2014)	Mineralogy	Mineralogy dominates, TOC is not considered	Not considered
Glorioso and Rattia (2011)	Mineralogy	Mineralogy dominates, TOC is a minor consideration	TOC should be considered in mineralogy brittleness method. Maturation is not considered.
Alzahabi et al. (2015)	Mineralogy	Mineralogy dominates, TOC is not considered	Not considered
Grieser and Bray (2007)	Elastic	Mineralogy dominates, TOC is considered	Higher TOC correlates to more **ductile** behavior. Maturation is not considered.
Rickman et al. (2008)	Elastic	Pore Pressure and Fluid Effects dominates, mineralogy is considered, TOC is not considered	Not considered
Wilson et al. (2017)	Elastic	Mineralogy dominates, TOC is considered	Higher TOC correlates to more **ductile** behavior. Maturation is not considered.
Mondol (2018)	Elastic	Mineralogy dominates, TOC is considered	Higher TOC correlates to more **brittle** behavior. Maturation is not considered.
Present study	Elastic	TOC and Maturation, mineralogy, pore pressure, and fluid effects considered	Higher TOC correlates to more **brittle** behavior. Lower values of TOC will prolong **ductile** behavior during maturation.

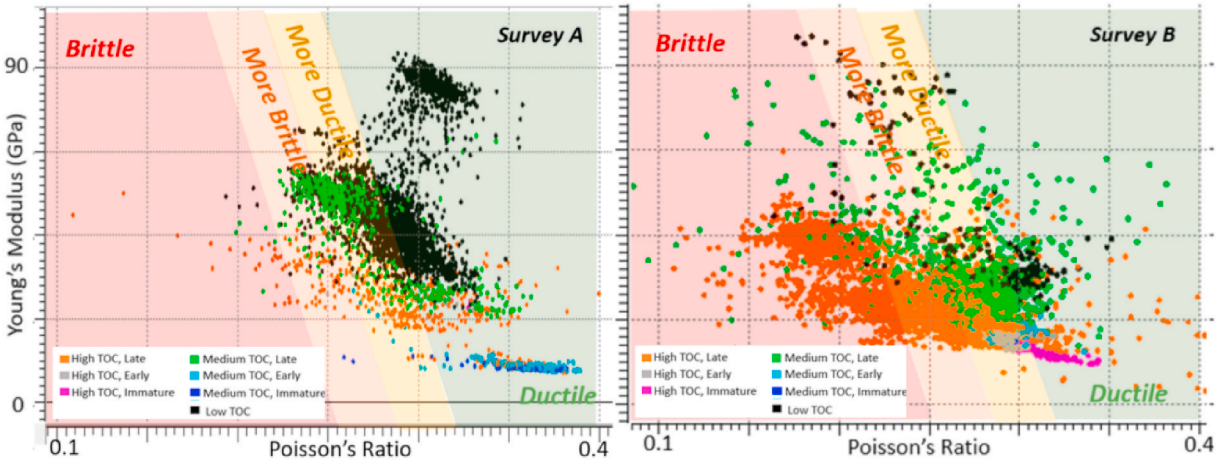

Fig. 15. Results of the Organic Maturation Product (OMP) with a geomechanical template, Young's modulus and Poisson's ratio for both Surveys A and B (from well data), with the organic maturation product (OMP) template that captures both the TOC range and the maturation stage, distributed across the background brittleness index from Perez and Marfurt (2014). Data clearly show a difference in the maturation levels for Survey A and Survey B.

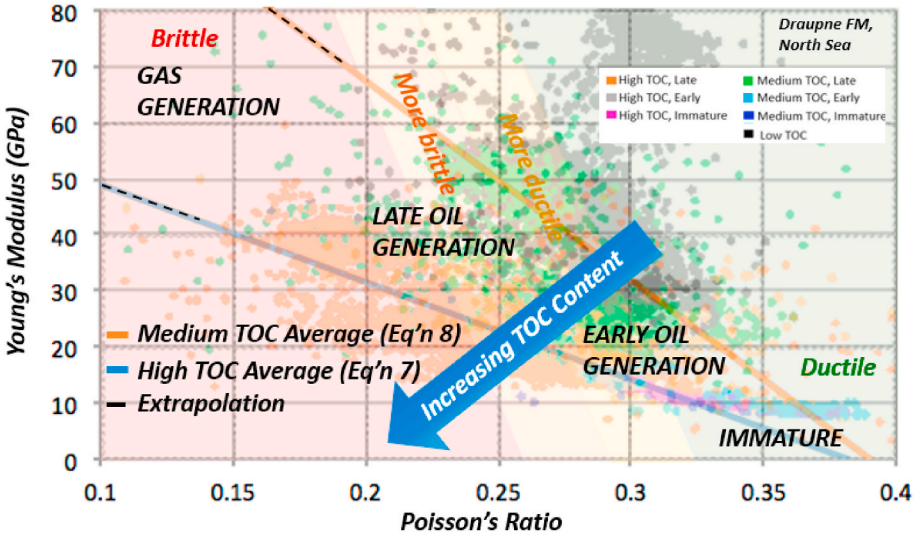

Fig. 16. Organic maturation product (OMP) rock physics template: This template explores how maturation and TOC impact shale brittleness and ductility in the Draupne Formation, the central North Sea. Both TOC and maturation play a significant role, with high TOC shale quickly becoming brittle as it moves from immature towards gas generation. Medium TOC shale, in contrast, moves more slowly from ductile to more brittle between immature and late oil generation. Finally, low TOC rocks have little to no maturation and tend to plot in the ductile region. The blue arrow indicates increasing TOC content. The blue and orange lines indicate trendlines for the average high and medium TOC shales (Equations (10) and (11)). Black dashed lines indicate the domain where these lines have been extrapolated into the gas generation window. (For interpretation of the references to color in this figure legend, the reader is referred to the Web version of this article.)

correlates to Poisson's ratio once porosity has been accounted for. The relationship between TOC and geomechanical properties is further modified by what stage of maturation the shale is currently at. Organic-rich shale with high TOC will quickly grade from ductile into brittle behavior as it matures. In our data, it is defined by the following relationship (Equation (10)):

$$E = -172.2\upsilon + 66.3 \tag{10}$$

where E is Young's modulus (in GPa), and υ is Poisson's ratio (unitless). Contrasting this, an organic-rich shale with medium TOC will progress much more slowly from ductile into brittle behavior. It is defined by the following relationship (Equation (11)):

$$E = -356.3\upsilon + 139.5 \tag{11}$$

These equations are based on the average geomechanical values for high and medium TOC rocks given by the relationships shown in Fig. 16 from both Survey A and B. Since seismic datasets have significantly more data points than well log datasets, the seismic facies dataset was decimated while preserving the trend. It has already been shown that what is true for the petrophysical results is also shown for the inversion results (Fig. 3). Relatively immature rocks plot in the same region despite very different TOC concentrations. This stands in stark contrast to organic-rich shales that have undergone significant maturation, which show a larger difference in geomechanical values depending on the TOC levels. Where gas generation would occur was extrapolated for both curves (black dashed lines in Fig. 16). Increases in TOC also result in a greater uncertainty based on the scatter from the dataset of our study. While there is a possible range for low TOC rocks as well, they were not taken into account for this study.

The proposed OMP template (Fig. 16) represents a novel way to quantify how shale's organic content, in combination with how it matures, impacts its geomechanical parameters. It can be seen that low TOC shales will typically plot within a ductile range, only reaching a more brittle nature under comparatively higher temperature and pressure. In stark contrast to this, a TOC-rich shale will progress relatively rapidly from ductile into brittle, even prior to reaching temperatures and pressures concurrent with gas generation. Shales with neither high nor low TOC are bounded by these two extremes. Therefore, it is expected that shales with greater TOC will result in better mobilization of hydrocarbons because their brittle behavior may allow fractures to propagate and remain open. Note that the results also highlight areas where vastly different rock in terms of TOC and maturation could behave mechanically the same, i.e., a late oil generation rock of medium TOC should behave mechanically similar to an early oil generation rock with high

TOC.

Furthermore, depending on various factors, including possible TOC variation, maturation, and mineralogy, rocks along the medium TOC average curve and the high TOC average curve could have similar mechanical behavior to rocks with low TOC. Utilization of the OMP rock physics template provides a relationship for the impact of variable levels of both TOC and maturation for forward modeling of organic-rich shale. When used for a potential source rock, it may inform as to the quality thereof; however, it could also be used for caprock to help guide interpretation as to its suitability for the play. Furthermore, the results act as verification of laboratory measurements showing the relationship between the maturation of kerogen (Prasad et al., 2009, 2011; Zargari et al., 2013, 2016) and their geomechanical behavior.

6. Conclusions

We introduce a rock physics template, the Organic Maturation Product that classifies semi-quantitatively how the nature of the shale's geomechanical properties evolve with variations in both TOC content and kerogen maturation. This template is built from a comprehensive dataset (3D seismic data, well-logs, geochemical analyses) acquired in the Draupne Formation, a major source rock in the North Sea. Specifically, higher TOC encourages a faster transition from ductile to brittle behavior during the maturation process. This template helps explain how different interpretations of this relationship could exist within the literature. Use of the rock physics template is ideal for better understanding shale as a source rock within an exploration play.

Multiple end-member depositional models exist to explain TOC. We used a combination of arbitrary cross-sections and stratal slices to demonstrate how TOC distribution in the Draupne Formation source rock shale may have been impacted by deposition, with a focus on known depositional environments for the study area in the North Sea. Two depositional models fit the patterns found in the 3D seismic data – submarine debris flows and pelagic deposits. The study confirms a relationship between depth, maturation, and compaction, wherein increased depth correlates positively with maturation and compaction. Deviations from this are explained by the fact that relatively immature organic-rich shale will contain kerogen that is load-bearing. Deviations from the background trend also occurred proximal to salt diapirs, resulting in greater maturation. The typical Draupne Formation distribution for TOC is present and is confirmed by the inversion results.

Declaration of competing interest

The authors declare that they have no known competing financial interests or personal relationships that could have appeared to influence the work reported in this paper.

Acknowledgements

We thank the Norwegian Research Council for providing funding (RCN no. 267775). Further, thanks for helpful conversations are extended to Maya Kobchenko, Austin Bailey, Andrew Johnson, Manzar Fawad and Celine Brun-Lie. Data is made available through the public databases DISKOS (https://portal.diskos.cgg.com/whereoil-data/) and NPD (https://factpages.npd.no/en/wellbore). Academic software licenses have been provided by Lloyd's Register for Interactive Petrophysics, CGG for both Jason and Hampson-Russell, and Schlumberger for Petrel.

References

Alzahabi, A., AlQahtani, G., Soliman, M.Y., Bateman, R.M., Asquith, G., Vadapalli, R., 2015. Fracturability index is a mineralogical index: a new approach for fracturing decision. In: SPE Saudi Arabia Section Annual Technical Symposium and Exhibition. Society of Petroleum Engineers.

Anders, M.H., Laubach, S.E., Scholz, C.H., 2014. Microfractures: a review. J. Struct. Geol. 69, 377–394. https://doi.org/10.1016/j.jsg.2014.05.011. Part B.

Antoine, J.W., Bryant, W.R., 1969. Distribution of salt and salt structures in Gulf of Mexico. AAPG (Am. Assoc. Pet. Geol.) Bull. 53, 2543–2550. https://doi.org/10.1306/5D25C973-16C1-11D7-8645000102C1865D.

Arthur, M.A., Sageman, B.B., 1994. Marine black shales: depositional mechanisms and environments of ancient deposits. Annu. Rev. Earth Planet Sci. 22, 499–511. https://doi.org/10.1146/annurev.ea.22.050194.002435.

Avseth, P., Carcione, J.M., 2015. Rock-physics analysis of clay-rich source rocks on the Norwegian Shelf. Lead. Edge 34, 1340–1348. https://doi.org/10.1190/tle34111340.1.

Avseth, P., Mavko, G., Dvorkin, J., Mukerji, T., 2001. Rock Physics of Seismic Properties of Sands and Shales as a Function of Burial Depth: 2001 SEG Annual Meeting. SEG. https://doi.org/10.1190/1.1816471.

Baig, I., Faleide, J.I., Mondol, N.H., Jahren, J., 2019. Burial and exhumation history controls on shale compaction and thermal maturity along the Norwegian North Sea basin margin areas. Mar. Petrol. Geol. 104, 61–85. https://doi.org/10.1016/j.marpetgeo.2019.03.010.

Baldwin, B., Butler, C.O., 1985. Compaction curves 1. AAPG (Am. Assoc. Pet. Geol.) Bull. 69, 622–626.

Banerjee, A., Sinha, A.K., Jain, A.K., Thomas, N.J., Misra, K.N., Cahndra, K., 1998. A mathematical representation of Rock-Eval hydrogen index vs. Tmax profiles. Organic Geochem. 28, 43–55. https://doi.org/10.1016/S0146-6380(97)00119-8.

Baytok, S., Pranter, M.J., 2013. Fault and fracture distribution within a tight-gas sandstone reservoir: mesaverde group, mamm creek field. Piceance Basin, Colorado, USA: Petrol. Geosci. 19, 203–222. https://doi.org/10.1144/petgeo2011-093.

Beaumont, E.A., Foster, N.H., 1999. Exploring for Oil and Gas Traps: AAPG Treatise Handbook.

Blakey, R.C., Middleton, L.T., 1983. Permian shoreline eolian complex in central Arizona: dune changes in response to cyclic sea level changes: developments in. Sedimentology 38, 551–581.

Bourg, I.C., 2015. Sealing shales versus brittle shales: a sharp threshold in the material properties and energy technology uses of fine-grained sedimentary rocks. Environ. Sci. Technol. Lett. 2, 255–259. https://doi.org/10.1021/acs.estlett.5b00233.

Broadhead, M., 2016. The effect of TOC on acoustic impedance for a Middle Eastern source rock. Lead. Edge 35, 258–264. https://doi.org/10.1190/tle35030258.1.

Bugge, T., Tveiten, B., Backstrom, S., 2001. The Depositional History of the Cretaceous in the Northeastern North Sea, vol. 10. Norwegian Petroleum Society Special Publications, pp. 279–291. https://doi.org/10.1016/S0928-8937(01)80018-7.

Castagna, J.P., Batzle, M.L., Eastwood, R.L., 1985. Relationship between compressional-wave and shear-wave velocities in clastic silicate rocks. Geophysics 50, 571–581. https://doi.org/10.1190/1.1441933.

Chauve, T., Scholtès, L., Donzé, F., Mondol, N.H., Renard, F., 2020. Layering in shales controls microfracturing at the onset of primary migration in source rocks. J. Geophys. Res. 125, e2020JB019444 https://doi.org/10.1029/2020JB019444.

Cook, J., 1999. The effects of pore pressure on the mechanical and physical properties of shales. Oil Gas Sci. Technol. 54, 695–701. https://ogst.ifpenergiesnouvelles.fr/articles/ogst/pdf/1999/06/cook_v54n6.pdf.

Cox, D.R., Newton, A.M.W., Huuse, M., 2020. An introduction to seismic reflection data: acquisition, processing, and interpretation. In: Cox, D.R., Newton, A.M.W., Huuse, M. (Eds.), Regional Geology and Tectonics, pp. 571–603. https://doi.org/10.1016/B978-0-444-64134-2.00020-1.

Cooke, I.L, 2014. User guide total organic carbon (TOC) dataset: British Geological Survey (BGS) Internal Report. http://nora.nerc.ac.uk/id/eprint/509720/1/OR14056.pdf.

Craddock, P.R., Bake, K.D., Pomerantz, A.E., 2018. Chemical, molecular, and microstructural evolution of kerogen during thermal maturation: case study from the Woodford Shale of Oklahoma. Energy Fuel. 32, 4859–4872. https://doi.org/10.1021/acs.energyfuels.8b00189.

Craddock, P.R., Mosse, L., Bernhardt, C., Ortiz, A.C., Tomassini, F.G., Saldungaray, P., Pomerantz, A.E., 2019. Characterization and range of kerogen properties in the Vaca Muerta formation Neuquen basin, Argentina. Org. Geochem. 129, 42–44. https://doi.org/10.1016/j.orggeochem.2019.01.016.

Daniilidis, A., Herber, R., 2017. Salt intrusions providing a new geothermal exploration target for higher energy recovery at shallower depths. Energy 118, 658–670. https://doi.org/10.1016/j.energy.2016.10.094.

Duenas, C., 2014. Understanding Rock Quality Heterogeneity of Montney Shale Reservoir, Pouce Coupe Field. M.S. Thesis, Colorado School of Mines, Alberta, Canada. https://mountainscholar.org/bitstream/handle/11124/441/Duenas_mines_0052N_10446.pdf?sequence=1.

Dutta, T., Mavko, G., Mukerji, T., 2009. Compaction trends for shale and clean sandstone in shallow sediments. Gulf of Mexico: Lead. Edge 28, 590–596. https://doi.org/10.1190/1.3124935.

Espitalie, J., Deroo, G., Marquis, F., 1985. La pyrolysis Rock-Eval etses applications. Oil Gas Sci. Technol. 40, 755–784. https://doi.org/10.2516/ogst:1985045.

Ewy, R., 2019. Claystone Porosity and Mechanical Behavior vs. Geologic Burial Stress: 6th EAGE Shale Workshop. EAGE. https://doi.org/10.3997/2214-4609.201900283.

Faleide, J.L., Tsikalas, F., Breivik, A.J., Mjelde, R., Ritzmann, O., Engen, O., Wilson, J., Eldhom, O., 2008. Structure and evolution of the continental margin off Norway and the Barents Sea. Episodes 31, 82–91. https://doi.org/10.18814/epiiugs/2008/v31i1/012.

Fjaer, E., Holt, R., Raaen, A., Risnes, R., Horsrud, P., 2008. Petroleum Related Rock Mechanics, vol. 53. Elsevier Science.

Fox, A., Snelling, P., McKenna, J., Neale, C., Neuhaus, C., Miskimmins, J., 2013. Geomechanical Principles for Unconventional Reservoirs. Microseismic. http://

www.microseismic.com/wpcontent/uploads/2017/07/2013_Geomechanical_Principles_For_Unconventional_Resources.pdf.
Galbraith, M., Hall, M., 1997. Some causes of artefacts in 3-D seismic surveys and strategies to minimize them. Explor. Geophys. 28, 63–65. https://doi.org/10.1071/EG997063.
Gardner, G.H., Gardner, L.W., Gregory, A.R., 1974. Formation velocity and density – the diagnostic basis for stratigraphic traps. Geophysics 39, 770–780. https://doi.org/10.1190/1.1440465.
Glorioso, J.C., Rattia, A., 2011. Unconventional reservoirs: basic petrophysical concepts for shale gas. In: Proceedings of the SPE/EAGE European Unconventional Resources Conference and Exhibition from Potential to Production. Vienna, Austria, 20–22 March 2012.
Gray, D., Anderson, P., Logel, J., Schmidt, D., Schmid, R., 2012. Estimation of stress and geomechanical properties using 3D seismic data. First Break 30, 59–68. https://doi.org/10.3997/1365-2397.2011042.
Grieser, B., Bray, J., 2007. Identifcation of production potential in unconventional reservoirs: 2007. SPE Production and Operations Symposium. https://doi.org/10.2118/106623-MS. SPE.
Haines, S.H., Plujim, B.A., Ikari, M.J., Saffer, D.M., Marone, C., 2009. Clay fabric intensity in natural and artificial fault gouges: implications for brittle fault zone processes and sedimentary basin clay fabric evolution. J. Geophys. Res. 114, B05406. https://doi.org/10.1029/2008JB005866.
Hansen, J.A., Yenwongfai, H.D., Fawad, M., Mondol, N.H., 2017. Estimating exhumation using experimental compaction trends and rock physics relations, with continuation into analysis of source and reservoir rocks: central North Sea, offshore Norway. In: 88th Annual International Meeting. Expanded abstracts, pp. 3971–3975.
Hansen, J.A., Mondol, N.H., Fawad, M., 2019. Organic content and maturation effects on elastic properties of source rock shales in the Central North Sea: Interpretation. https://doi.org/10.1190/INT-2018-0105.1, 7, 477-497.
Hansen, J.A., Mondol, N.H., Tsikalas, F., Faleide, J.I., 2020. Caprock characterization of Upper Jurassic organic-rich shales using acoustic properties. Norwegian Continental Shelf: Mar. Petrol. Geol. 121, 104603. https://doi.org/10.1016/j.marpetgeo.2020.104603.
Heslop, K.A., 2010. Generalized Method for the Estimation of TOC from GR and Rt: Search and Discovery Article. AAPG Technical Program Expanded Abstracts. No. 80117.
Holt, R.M., Fjaer, E., Stenebraten, J.F., Nes, O.M., 2015. Brittleness of shales: relevance to borehole collapse and hydraulic fracturing. J. Petrol. Sci. Eng. 131, 200–209. https://doi.org/10.1016/j.petrol.2015.04.006.
Horner, D.R., 1951. Pressure build-up in wells: third world petroleum congress. The Hague. https://www.zetaware.com/utilities/bht/horner.html, 34, 316.
Inichinbia, S., Sule, P.O., Ahmed, A.L., Hamza, H., Lawal, K.M., 2014. Petrophysical analysis of among hydrocarbon field fluid and lithofacies using well log data. J. Appl. Geol. Geophys. 2, 86–96. https://doi.org/10.9790/0990-02218696.
Isaksen, G.H., Ledje, H.I., 2001. Source rock quality and hydrocarbon migration pathways within the greater Utsira High area, Viking Graben, Norwegian North Sea. AAPG (Am. Assoc. Pet. Geol.) Bull. 85, 861–883. https://doi.org/10.1306/8626CA23-173B-11D7-8645000102C1865D.
Jackson, C.A.L., Kane, K.E., Larsen, E., 2010. Structural evolution of minibasins on the Utsira High, northern North Sea; implications for Jurassic sediment dispersal and reservoir distribution. Petrol. Geosci. 16, 105–120. https://doi.org/10.1144/1354-079309-011.
Jarvie, D.M., Hill, R.J., Ruble, T.E., Pollastro, R.M., 2007. Unconventional shale-gas systems: the Mississippian Barnett Shale of north-central Texas as one model for thermogenic shale-gas assessment. AAPG (Am. Assoc. Pet. Geol.) Bull. 91, 475–499. https://doi.org/10.1306/12190606068.
Jensen, P.K., 1983. Calculations on the thermal conditions around a salt diapir. Geophys. Prospect. 31, 481–489. https://doi.org/10.1111/j.1365-2478.1983.tb01064.x.
Jensen, P.K., 1990. Analysis of the temperature field around salt diapirs. Geothermics 19, 273–283. https://doi.org/10.1016/0375-6505(90)90047-F.
Jin, X., Shah, S.N., Roegiers, J.-C., Zhang, B., 2014. Fracability evaluation in shale reservoirs-an integrated petrophysics and geomechanics approach. In: SPE Hydraulic Fracturing Technology Conference. Society of Petroleum Engineers. https://doi.org/10.2118/168689-MS.
Johnson, J.R., 2017. Applications of Geostatistical Seismic Inversion to the Vaca Muerta, Neuquen Basin. Colorado School of Mines, Argentina. M.S. thesis. https://mountainscholar.org/bitstream/handle/11124/170976/Johnson_mines_0052N_11230.pdf?sequence=1.
Johnson, J.R., Renard, F., Mondol, N., 2021. Salt Remobilization Timing and its Impact on Two Norwegian Contentinental Shelf Organic-Rich Shale Formations. Geoconvention 2021. https://geoconvention.com/wp-content/uploads/abstracts/2021/67503-salt-removilization-timing-and-its-impact-on-two.n.pdf.
Kalani, M., Jahren, J., Mondol, N.H., Faleide, J.I., 2015. Petrophysical implications of source rock microfracturing. Int. J. Coal Geol. 143, 43–67. https://doi.org/10.1016/j.coal.2015.03.009.
Katsube, T.J., Williamson, M.A., 1994. Effects of diagenesis on shale nano-pore structure and implications for sealing capacity. Clay Miner. 29, 451–461. https://doi.org/10.1180/claymin.1994.029.4.05.
Kemper, M., Gunning, J., 2014. Joint impedance and facies inversion-seismic inversion redefined. First Break 32, 89–95. https://doi.org/10.3997/1365-2397.32.9.77968.
Kennedy, M., Mayer, L., 2019. Dominance of Wind Blown Minerals in Black Shales, Connecting Continentatl Climate, Fe Fertilization and Mineral Ballasting: 6th EAGE Shale Workshop. EAGE. https://doi.org/10.3997/2214-4609.201900282.
Kumar, N., Negi, S.S., 2012. Low frequency modeling and its impact on seismic inversion data. In: 9th Biennial International Conference and Exposition on Petroleum Geophysics. https://doi.org/10.3997/2214-4609.201702511.
Kuuskraa, V.A., Stevens, S.H., Moodhe, K., 2013. Technically Recoverable Shale Oil and Shale Gas Resources: an Assessment of 137 Shale Formations in 41 Countries outside the United States: U.S. Energy Information Administration. https://www.eia.gov/analysis/studies/worldshalegas/pdf/overview.pdf?zscb=79906188.
Løseth, H., Wensaas, L., Gading, M., Duffaut, K., Springer, M., 2011. Can hydrocarbon source rocks be identified on seismic data? Geology 39, 1167–1170. https://doi.org/10.1130/G32328.1.
MacFarlane, T.L., 2014. Amplitude Inversion of Fast and Slow Converted Waves for Fracture Characterization of the Montney Formation in the Pouce Coupe Field. Colorado School of Mines, Alberta, Canada. M.S. Thesis. https://mountainscholar.org/bitstream/handle/11124/10645/MacFarlane_mines_0052N_10560.pdf?sequence=1.
Magara, K., 1980. Comparison of porosity-depth relationships of shale and sandstone. J. Petrol. Geol. 3, 175–185. https://doi.org/10.1111/j.1747-5457.1980.tb00981.x.
Magri, F., Littke, R., Rodon, S., Bayer, U., Urai, J.L., 2008. Temperature fields, petroleum maturation and fluid flow in the vicinity of salt domes. In: Littke, R., Bayer, U., Gajewski, D., Nelskamp, S. (Eds.), Dynamics of Complex Intracontinental Basins: the Central European Basin System. Springer, pp. 323–344.
Mannie, A.S., Jackson, C.A.L., Hampson, G.J., 2014. Structural controls on the stratigraphic architecture of net-transgressive shallow-marine strata in a salt-influenced rift basin: middle-to-Upper Jurassic Egersund Basin. Norwegian North Sea: Basin Res. 26, 675–700. https://doi.org/10.1111/bre.12058.
Marfurt, K.J., Alves, T.M., 2014. Pitfalls and limitations in seismic attribute interpretation of tectonic features. Interpretation 3, 5–15. https://doi.org/10.1190/INT-2014-0122.1.
Mondol, N.H., 2018. Seal Quality Prediction Using E-Poisson's Ratio Rock Physics Template – A Case Study from the Norwegian Barents Sea: Geoconvention 2018. https://geoconvention.com/uploads/2018abstracts/241_GC2018_Seal_quality_prediction_using_E-v_rock_physics_templet.pdf.
Mondol, N.H., Bjørlykke, K., Jahren, J., Høeg, K., 2007. Experimental mechanical compaction of clay mineral aggregates—Changes in physical properties of mudstones during burial. Mar. Petrol. Geol. 24 (5), 289–311. https://doi.org/10.1016/j.marpetgeo.2007.03.006.
NPD, 2021. Norwegian Petroleum Directorate FactPages. http://factpages.npd.no/. (Accessed 6 November 2021).
Nooraiepour, M., Mondol, N.H., Hellevang, H., Bjorlykke, K., 2017. Experimental mechanical compaction of reconstituted shale and mudstone aggregates: investigation of petrophysical and acoustic properties of SW Barents Sea cap rock sequences. Mar. Petrol. Geol. 80, 265–292. https://doi.org/10.1016/j.marpetgeo.2016.12.003.
Nygård, R., Gutierrez, M., Bratli, R.K., Høeg, K., 2006. Brittle–ductile transition, shear failure and leakage in shales and mudrocks. Marine Petrol. Geol. 23, 201–212. https://doi.org/10.1016/marpetgeo.2005.10.001.
Olsen, H., Briedis, N.A., Renshaw, D., 2017. Sedimentological analysis and reservoir characterization of a multi-Darcy, billion barrel oil field – the Upper Jurassic shallow marine sandstones of the Johan Sverdrup field, North Sea, Norway. Mar. Petrol. Geol. 84, 102–134. https://doi.org/10.1016/j.marpetgeo.2017.03.029.
Ougier-Simonin, A., Renard, F., Boehm, C., Vidal-Gilbert, S., 2016. Microfracturing and microporosity in shales. Earth Sci. Rev. 162, 198–226. https://doi.org/10.1016/j.earscirev.2016.09.006.
Passey, Q.R., Creaney, S., Kulla, J.B., Moretti, F.J., Stroud, J.D., 1990. A practical model for organic richness from porosity and resistivity logs. AAPG (Am. Assoc. Pet. Geol.) Bull. 74, 1777–1794. https://doi.org/10.1306/0C9B25C9-1710-11D7-8645000102C1865D.
Passey, Q.R., Bohacs, K.M., Esch, W.L., Klimentidis, R., Sinha, S., 2012. My Source Rock Is Now My Reservoir – Geologic and Petrophysical Characterization of Shale-Gas Reservoirs: Search and Discovery Article. AAPG Technical Program Expanded Abstracts, No. 80231. http://www.searchanddiscovery.com/pdfz/documents/2012/80231passey/ndx_passey.pdf.html.
Pendrel, J., Debeye, H., Pedersen-Tatlovic, R., Goodway, B., Dufour, J., Bogaards, M., Stewart, R., 1999. Estimation and Interpretation of P and S-Impedance Volumes from Simultaneous Inversion of P-Wave Offset Seismic Data. SEG Technical Program Expanded Abstracts 2000. https://pdfs.semanticscholar.org/04a6/9f9803ce0f98a80d2d75a1a9a65998d4d2a3.pdf.
Pendrel, J., Mangat, C., Feroci, M., 2006. Using Bayesian inference to compute facies-fluid probabilities: CSPG-CSEG-CLWS 2006. https://cseg.ca/assets/files/resources/abstracts/2006/238S0131.pdf.
Perez, R., Marfurt, K., 2014. Mineralogy-based brittleness prediction from surface seismic data: application to the Barnett Shale. Interpretation 2, 1–17. https://doi.org/10.1190/INT-2013-0161.1.
Prasad, M., Pal-Bathija, A., Johnston, M., Rydzy, M., Batzle, M., 2009. Rock physics of the unconventional. Lead. Edge 28, 34–38. https://doi.org/10.1190/1.3064144.
Prasad, M., Kenechukwu, C., McEvoy, T.E., Batzle, M., 2011. Maturity and impedance analysis of organic-rich shales. SPE Reservoir Eval. Eng. 14, 533–543. https://doi.org/10.2118/123531-PA.
Rahman, M.D.J., Fawad, M., Mondol, N.H., 2020. Organic-rich shale caprock properties of potential CO2 storage sites in the northern North Sea, offshore Norway. Mar. Petrol. Geol. 122, 104665. https://doi.org/10.1016/j.marpetgeo.2020.104665.
Reading, H.G., Richards, M., 1994. Turbidite system in deep-water basin margins classified by grain size and feeder system. AAPG (Am. Assoc. Pet. Geol.) Bull. 78, 792–822. https://doi.org/10.1306/A25FE3BF-171B-11D7-8645000102C1865D.
Rickett, J.E., Lumley, D.E., 1999. Cross-equalization data processing for time-lapse seismic reservoir monitoring: a case study from the Gulf of Mexico. Geophysics 66, 1015–1025. https://doi.org/10.1190/1.1487049.

Rickman, R., Mullen, M., Petre, E., Grieser, B., Kundert, D., 2008. A Practical Use of Shale Petrophysics for Stimulation Design Optimization: All Shale Plays Are Not Clones of the Barnett Shale. Society of Petroleum Engineers, Richardson, TX, USA.
Robertson, E.C., 1988. Thermal Properties of Rocks. US Department of the Interiror Geological Survey. https://doi.org/10.3133/ofr88441. Open-File Report 88-441.
Rossland, A., Escalona, A., Rolfsen, R., 2013. Permian-Holocene Tectonostratigraphic Evolution of the Mandal High, Central Graben, North Sea: AAPG Bulletin, 97, 923 – 957.
Russell, B.H., 1988. Introduction to Seismic Inversion Methods: SEG. https://doi.org/10.1190/1.9781560802303.
Sadeghtabaghi, Z., Talebkeikhah, M., Rabbani, A.R., 2020. Prediction of vitrinite reflectance values using machine learning techniques: a new approach. J. Petrol. Explor. Prod. Technol. 11, 651–671. https://doi.org/10.1007/s13202-020-01043-8.
Sayers, C.M., Dasgupta, S., 2019. A predictive anisotropic rock-physics model for estimating elastic rock properties of unconventional shale reservoirs. Lead. Edge 38, 358–365. https://doi.org/10.1190/tle38050358.1.
Schmoker, J.W., Hester, T.C., 1983. Organic carbon in Bakken formation, United States portion of Williston basin. AAPG (Am. Assoc. Pet. Geol.) Bull. 67, 2165–2174. https://doi.org/10.1306/AD460931-16F7-11D7-8645000102C1865D.
Sheriff, R., 2002. Encyclopedic dictionary of applied geophysics: SEG. https://doi.org/10.1190/1.9781560802969.
Skurtveit, E., Miri, R., Hellevang, H., 2018. Geological Carbon Storage: Subsurface Seals and Caprock Integrity. American Geophysical Union. https://doi.org/10.1002/9781119118657.
Somoza, A.V., Waters, K., Kemper, M., 2015. Improved Seismic Inversion and Facies Using Regional Rock Physics Trends: Case Study from the Central North Sea: EAGE. 3rd workshop on Rock Physics, pp. 1–5. https://doi.org/10.3997/2214-4609.201414389.
Sonnenberg, S.A., 2011. TOC and pyrolysis data for the Bakken shales, Williston basin, north Dakota and Montana. In: Robinson, J.W., LeFever, J.A., Gaswirth, S.B. (Eds.), Bakken-Three Forks Petroleum System in the Williston Basin. Rocky Mountain Association of Geologists, pp. 308–331.
Sonnenberg, S.A., Meckel, L., 2017. Our Current Working Model for Unconventional Tight Petroleum Systems: Oil and Gas: Search and Discovery. AAPG. http://www.searchanddiscovery.com/documents/2017/80589sonnenberg/ndx_sonnenberg.pdf. (Accessed 17 March 2021).
Soto, J.I., Hudec, M.R., Mondol, N.H., Heidari, M., 2021. Shale transformations and physical properties – implcations for seismic expression of mobile shales. Earth Sci. Rev. 220, 103746. https://doi.org/10.1016/j.earscirev.2021.103746.
Steiner, S., Ahsan, S.A., Raina, I., Dasgupta, S., Lis, G.P., 2016. Interpreting total organic carbon TOC in source rock oil plays. In: SPE International Petroleum Exhibition and Conference. https://doi.org/10.2118/183050-MS.
Stow, D.A., Mayall, M., 2000. Deep-water sedimentary system: new models for the 21st century. Mar. Petrol. Geol. 17, 125–135. https://doi.org/10.1016/S0264-8172(99)00064-1.
Thomsen, L., 1990. Poisson was not a geophysicist. Lead. Edge 9, 27–29. https://doi.org/10.1190/1.1439706.
Thomsen, L., 1996. Poisson was not a rock physicist, either. Lead. Edge 15, 793–880. https://doi.org/10.1190/1.1437382.
Thyberg, B., Jahren, J., Winje, T., Bjørlykke, K., Faleide, J., 2009. From mud to shale: rock stiffening by microquartz cementation. First Break 27, 2. https://doi.org/10.3997/1365-2397.2009003.
Thyberg, B., Jahren, J., Winje, T., Bjorlykke, K., Faleide, J.I., Marcussen, O., 2010. Quartz cementation in Late Cretaceous mudstones, northern North Sea: Changes in rock properties due to dissolution of smectite and precipitation of miro-quartz crystals. Mar. Petrol. Geol. 27, 1752–1764. https://doi.org/10.1016/j.marpetgeo.2009.07.005.
Tissot, B.P., Welte, D.H., 1984. Petroleum Formation and Occurrence. Springer-Verlag Berlin Heidelberg GmbH.
Vernik, L., 2016. Seismic Petrophysics in Quantitative Interpretation: Investigation in Geophysics, vol. 18. SEG, Tulsa, Oklahoma.
Vernik, L., Landis, C., 1996. Elastic anisotropy of source rocks – implications for hydrocarbon generation and primary migration. AAPG (Am. Assoc. Pet. Geol.) Bull. 80, 531–544. https://doi.org/10.1306/64ED8836-1724-11D7-8645000102C1865D.
Ward, J., 2010. Kerogen density in the marcellus shale, SPE unconventional gas conference. https://doi.org/10.2118/131767-MS.
Welte, D.H., Horsfield, B., Baker, D.R., 1997. Petroleum and Basin Evolution, Insights from Petroleum Geochemisty, Geology, and Basin Modeling. Springer.
Whipp, P.S., Jackson, C.A.-L., Gawthorpe, R.L., Dreyer, T., Quinn, D., 2014. Normal fault array evolution above a reactivated rift fabric; a subsurface example from the northern Horda Platform. Norwegian North Sea: Basin Res. 26, 523–549. https://doi.org/10.1111/bre.12050.
Wilson, M.P., Worrall, F., Davies, R.J., Hart, A., 2017. Shallow aquifer vulnerability from subsurface fluid injection at a proposed shale gas hydraulic fracturing site. Water Resour. Res. 53, 9922–9940. https://doi.org/10.1002/2017WR021234.
Wu, Y., Ji, L., He, C., Zhang, Z., Zhang, M., Sun, L., Su, L., Xia, Y., 2016. The effects of pressure and hydrocarbon expulsion on hydrocarbon generation during hydrorous pyrolysis of type-I kerogen in source rock. J. Nat. Gas Sci. Eng. https://doi.org/10.1016/j.jngse.2016.08.0171875-5100.
Yenugu, M., Han, D., 2013. Seismic Characterization of Kerogen Maturity: an Example from Bakken Shale. SEG Technical Program Expanded Abstracts. https://doi.org/10.1190/segam2013-0629.1.
Yenwongfai, H., Mondol, N.H., Lecomte, I., Faleide, J.I., Leutscher, J., 2019. Integrating facies-based Bayesion inversion and supervised machine learning for petro-facies characterization in the Snadd Formation Goliat Field, south-western Barents Sea. Geophys. Prospect. 67, 1020–1039. https://doi.org/10.1111/1365-2478.12654.
Yilmaz, O., 2001. Seismic Data Analysis: Processing, Inversion, and Interpretation of Seismic Data: SEG. https://doi.org/10.1190/1.9781560801580.
Zadeh, M.K., Mondol, N.H., Jahren, J., 2017. Velocity anisotropy of Upper Jurassic organic-rich shales. Norwegian Continental Shelf: Geophysics 82, 61–75. https://doi.org/10.1190/geo2016-0035.1.
Zargari, S., Prasad, M., Kenechukwu, C., Mattson, E.D., 2013. Organic maturity, elastic properties, and textural characteristics of self resourcing reservoirs. Geophysics 78, 223–235. https://doi.org/10.1190/geo2012-0431.1.
Zargari, S., Wilkinson, T.M., Packard, C.E., Prasad, M., 2016. Effect of thermal maturity on elastic properties of kerogen. Geophysics 81, 1942–2156. https://doi.org/10.1190/geo2015-0194.1.
Ziegler, P.A., 1992. North Sea rift system. Tectonophysics 208, 55–75. https://doi.org/10.1016/0040-1951(92)90336-5.
Zoback, M., 2007. Reservoir Geomechanics. Cambridge University Press. https://doi.org/10.1017/CBO9780511586477.